INSTITUTE OF PHYSICS PUBLISHING INVERSE PROBLEMS

Inverse Problems **22** (2006) 1705–1729 doi:10.1088/0266-5611/22/5/011

Synthetic-aperture inversion in the presence of noise and clutter

Birsen Yazıcı[1], **Margaret Cheney**[2] **and Can Evren Yarman**[1]

[1] Department of Electrical, Computer and System Engineering, Rensselaer Polytechnic Institute, Troy, NY 12180-3590, USA
[2] Department of Mathematical Sciences, Rensselaer Polytechnic Institute, Troy, NY 12180-3590, USA

E-mail: yazici@ecse.rpi.edu

Received 4 January 2006, in final form 14 July 2006
Published 30 August 2006
Online at stacks.iop.org/IP/22/1705

Abstract

This paper presents an analytic method for synthetic-aperture inversion when the measurements are corrupted with noise and clutter. We use microlocal analysis in a statistical setting to develop filtered-backprojection-type reconstruction methods. The inversion method is applicable in non-ideal scenarios, such as those involving arbitrary source trajectories or variable antenna beam patterns. We show that the backprojection preserves the location and orientation of the singularities of the first- and second-order statistics of the target scene. We derive backprojection filters with respect to different statistical criteria. In particular, if we use a criterion based on first-order statistics, the resulting image can be interpreted as approximately unbiased. Alternatively, if we use a criterion based on second-order statistics to design the backprojection filter, such as a minimum-mean-square error criterion, the strength of the singularities due to noise and clutter is suppressed in the resulting image. Although we have developed our approach specifically for synthetic-aperture radar application, the method is also applicable to other inversion problems in which microlocal techniques are relevant, such as geophysics and x-ray tomography.

1. Introduction

Synthetic-aperture radar (SAR) imaging systems [1–6] form images from backscattered electromagnetic waves measured along the antenna flight trajectory (see figure 1).

Reconstruction algorithms for SAR are well known [1, 4, 5], at least for straight flight trajectories and systems whose antennas are able to form a narrow beam. Less well known are algorithms for systems with nonlinear flight trajectories, such as might be used by uninhabited

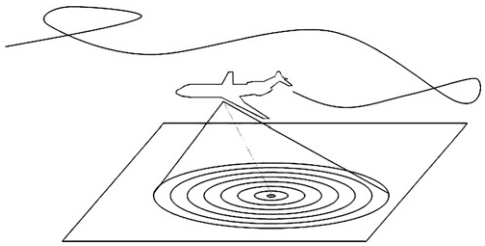

Figure 1. Acquisition geometry for SAR.

aerial vehicles (UAVs) operating in an unfriendly environment, and algorithms for wide-angle systems, such as staring radar and systems with poor directivity. Examples of the latter include low-frequency foliage-penetrating systems [6, 7], where the antenna footprint is large and standard narrow-beam imaging methods are not useful. The analysis of this paper encompasses all these scenarios.

In [8, 9], we developed an approximate analytic image reconstruction method for SAR based on microlocal analysis. Microlocal analysis is a theory for dealing with oscillatory integrals and singularities [10–18]. Microlocal analysis gives rise to filtered-backprojection-type reconstruction formulae, which have a number of advantages: (1) they are direct (non-iterative) methods, (2) they can account explicitly for factors such as the arbitrary flight trajectory, non-flat ground topography, antenna beam pattern, transmitted waveforms and geometric spreading and (3) they also have the desirable property that visible edges in the scene will appear in the image in the correct location and orientation.

Other researchers have also proposed edge-preserving reconstruction algorithms for SAR [19, 20]. These approaches, while resulting in images that are more easily interpretable, typically rely on iterative optimization schemes and are computationally intensive [21]. For these and other reasons that will become clear, the microlocal approach is an attractive alternative.

While the microlocal approach results in an approximate reconstruction, in practice the formulae often reduce to the exact inversion formulae that are known for idealized cases. This is the case here: our reconstruction formula reduces to the exact inversion formula of [22–24] for the case of a perfect point source moving along a straight flight track above a flat earth.

Microlocal reconstruction techniques have been used to advantage in the geophysics community, where the resulting algorithms have been found to be fast and robust [13, 15]. However, until now microlocal techniques have been developed and applied only in a deterministic setting; in this paper, we show how to combine microlocal analysis with a statistical formulation. In particular, we show how to use statistical considerations to choose a backprojection filter that suppresses clutter and noise and we analyse the properties of the resulting inversion formulae using microlocal analysis.

The significance of this paper is thus twofold: on a theoretical level we show how microlocal analysis can be combined with statistics; on a more applied level we develop an edge-preserving SAR imaging algorithm that can suppress clutter and noise. Moreover, because our physics-based approach incorporates arbitrary flight trajectories, beam patterns and transmitted waveforms, the resulting theory provides a design tool for these aspects of SAR systems. Although we have carried out the development specifically for SAR, the ideas are also applicable to other inversion problems in which microlocal techniques are relevant, such as geophysics and x-ray tomography.

Our study starts in section 2 with a physics-based forward model that can be used to model the antenna beam pattern, transmitted waveform and geometric spreading factors. We assume that the scene has a spatially varying mean value and that its second-order statistics are not necessarily stationary. In section 3, we introduce the backprojection operator and show that it puts the singularities of the first-order statistics of the scene in the correct location and orientation in the reconstructed image. In section 3.2, we consider two different ways to choose the backprojection filter. The first choice, which is typically used in the deterministic framework [15], results in an image in which the singularities of the first-order statistics appear as accurately as possible. This choice has the disadvantage that target singularities may be difficult to distinguish from those due to clutter and noise. This motivates an alternative criterion for choosing the backprojection filter, namely to minimize either the mean-square error between the reconstructed image and the scene or the closely related variance of the image. These choices have the effect of suppressing noise and clutter relative to the target. When the second-order statistics of the scene, noise and clutter are stationary, we obtain an explicit filter minimizing the total variance of the error. This filter can be viewed as an adaptive time-varying Wiener filter which varies with respect to location on the flight trajectory and the point reconstructed in the image. When the statistics are not stationary, we obtain an integral equation that must be solved to find the appropriate filter. When there is no noise and clutter, our inversion formula reduces to the deterministic one presented in [9]. Finally, section 4 presents numerical simulations to illustrate the theoretical results and to evaluate the performance of the reconstruction algorithms. We also include an analysis of the computational complexity of our algorithm. Section 5 summarizes our results and conclusion. The paper concludes with appendix A which gives a brief overview on microlocal analysis and image formation.

2. Physics-based SAR forward model

We discuss our approach in the specific context of SAR, although very similar ideas apply in a wide variety of other imaging problems that involve wave propagation.

2.1. A model for the ideal received signal

We model the received signal f as follows [8]. We assume that the scattering takes place on a known surface, which we parametrize by $\boldsymbol{x} \in \mathbb{R}^2$. (This assumption may be inappropriate for some situations, such as foliage-penetrating scenarios.) We denote by $\boldsymbol{r}_{s,\boldsymbol{x}}$ the vector from the antenna, located at known position $\boldsymbol{\gamma}(s)$, to the point on the ground parametrized by $\boldsymbol{x}$. We denote the target reflectivity function at $\boldsymbol{x}$ by $T(\boldsymbol{x})$.

We model scattering from the scene with the single-scattering (Born) approximation. This approximation is universally used in radar imaging; however, there are certainly cases where it is inappropriate and results in recognizable image artefacts [25]. Developing radar imaging methods to accommodate multiple scattering is an area of active research [26].

Under the Born approximation, ideal SAR measurements without noise and clutter can be modelled as

$$\tilde{f}(s,t) \approx \mathcal{F}[T](s,t) := \int \mathrm{e}^{-\mathrm{i}2\pi\omega(t-2|\mathbf{r}_{s,x}|/c)} A(\boldsymbol{x},s,\omega) T(\boldsymbol{x})\,\mathrm{d}\omega\,\mathrm{d}\boldsymbol{x}, \tag{1}$$

where c denotes the speed of light and A is a (complex) amplitude that includes the antenna beam pattern, the transmitted waveform, geometrical spreading factors, etc. Here t denotes (fast) time, ω is angular frequency and $2|\boldsymbol{r}_{s,\boldsymbol{x}}|/c$ is interpreted as the two-way travel time between the antenna at position parametrized by s and scattering point parametrized by $\boldsymbol{x}$.

We assume that for some m_A, A satisfies the *symbol* estimate given in [8]:

$$\sup_{(s,\boldsymbol{x})\in K}\left|\partial_\omega^\alpha\partial_s^\beta\partial_{x_1}^{\rho_1}\partial_{x_2}^{\rho_2}A(\boldsymbol{x},s,\omega)\right|\leqslant C_0(1+\omega^2)^{(m_A-|\alpha|)/2} \tag{2}$$

where K is any compact subset of $\mathbb{R}\times\mathbb{R}^2$ and the constant C_0 depends on K, α, β, ρ_1 and ρ_2. This assumption is needed in order to make various stationary phase calculations hold; in fact this assumption makes the 'forward' operator $\mathcal{F}$ a *Fourier integral operator* [10, 11, 12].

Note that for practical systems, which always have limited bandwidth, the integral expression (1) can be defined in the L^2 sense. Our image formation algorithm below, however, is motivated by an idealized high-frequency approximation.

The ideal inverse problem is to estimate T from knowledge of $\tilde{f}(s,t)$ for some range of s and t.

In general, the strategy for estimating T is to apply to the data $\mathcal{F}[T]$ an imaging operator $\mathcal{K}$. The estimate $\hat{T}$ for the target can thus be written as $\hat{T}=\mathcal{K}\mathcal{F}[T]$. (Note that we use hats both for estimated quantities and for unit vectors; the meaning is clear from the context.) The operator $\mathcal{L}=\mathcal{K}\mathcal{F}$ contains the information about how our estimate $\hat{T}$ is related to the actual target T. The kernel of $\mathcal{L}$ is called the *point spread function* or *ambiguity function*; we call the corresponding operator $\mathcal{L}$ the *image fidelity operator*. Our strategy is to determine $\mathcal{K}$ so that the image fidelity operator $\mathcal{L}=\mathcal{K}\mathcal{F}$ has desirable properties.

2.2. *Formulation of the SAR inverse problem in the presence of noise and clutter*

One of the fundamental problems in radar is the ubiquitous presence of noise and clutter in sensor measurements. Therefore, we extend the model in (1) to include clutter and noise.

We use the term 'clutter' for unwanted ground reflections. Thus, we model the measurements at the sensor as

$$d(s,t)=\mathcal{F}[T+C](s,t)+n(s,t), \tag{3}$$

where C denotes the reflectivity function of unwanted scatterers and $n(s,t)$ denotes the receiver noise. We note that the clutter process $\mathcal{F}C$ is a waveform-dependent process [27].

We make the following assumptions about the first-order statistics of the target, clutter and noise:

$$E[T(\boldsymbol{x})]=\mu(\boldsymbol{x}), \tag{4}$$

$$E[C(\boldsymbol{x})]=0, \tag{5}$$

$$E[n(s,t)]=0, \tag{6}$$

where E denotes the expected value. Note that the mean value $\mu(\boldsymbol{x})$ of the target scene $T(\boldsymbol{x})$ is not necessarily spatially constant. We define target, clutter and noise autocovariance, respectively, as

$$\mathcal{C}_T(\boldsymbol{x},\boldsymbol{x}'):=E[(T(\boldsymbol{x})-\mu(\boldsymbol{x}))\overline{(T(\boldsymbol{x}')-\mu(\boldsymbol{x}'))}], \tag{7}$$

$$\mathcal{R}_C(\boldsymbol{x},\boldsymbol{x}'):=E[C(\boldsymbol{x})\overline{C(\boldsymbol{x}')}], \tag{8}$$

$$\mathcal{R}_n(s,t;s',t'):=E[n(s,t)\overline{n(s',t')}]. \tag{9}$$

We assume that the target, clutter and noise are mutually statistically independent. We make the assumption that the variances $\mathcal{C}_T(\boldsymbol{x},\boldsymbol{x})<+\infty$, $\mathcal{R}_C(\boldsymbol{x},\boldsymbol{x})<+\infty$ and $\mathcal{R}_n(s,t;s,t)<+\infty$ and define all integrals involving T, C, n and d in the mean-square sense. Furthermore, we assume that the Fourier transforms of $\mathcal{C}_T$, $\mathcal{R}_C$ and $\mathcal{R}_n$ exist.

We will refer to T as the target scene, C as the clutter scene and $T + C$ as the scene. We will refer to the estimate $\hat{T}$ (see (10)) as the target image or image for short.

Our objective is to estimate the target scene T from the measurements $d(s, t)$, for some range of s and t, given $\mathcal{C}_T$, $\mathcal{R}_C$ and $\mathcal{R}_n$.

3. Image formation in the presence of noise and clutter

In this paper, we extend reconstruction techniques based on microlocal analysis [9, 13, 15] to a statistical setting. Such an approach is not only applicable to SAR, but can also benefit sonar, ultrasound and geophysical imaging problems.

The microlocal-analysis-based reconstruction method can be viewed as a *generalized filtered-backprojection* method where the data are first filtered and then backprojected. The key idea is that backprojection results in an image in which edges appear in the correct location and correct orientation.

We use the following backprojection operator $\mathcal{K}$ to form an image $\hat{T}$ of the target:

$$\hat{T}(z) := (\mathcal{K}d)(z) := \int Q(z, s, \omega)\, \mathrm{e}^{\mathrm{i}2\pi\omega(t-2|\mathbf{r}_{s,z}|/c)} d(s, t)\, \mathrm{d}t\, \mathrm{d}s\, \mathrm{d}\omega, \tag{10}$$

where Q will be determined in section 3.2 and is assumed to satisfy a symbol estimate of the form [9]. The image $\hat{T}$ is then related to the true target T via

$$\hat{T} = \mathcal{K}d = \mathcal{K}[\mathcal{F}(T + C) + n] = \mathcal{K}\mathcal{F}(T + C) + \mathcal{K}n. \tag{11}$$

We start our analysis with a precise statement of how the statistics of the scene and noise are mapped by the image fidelity operator $\mathcal{K}\mathcal{F}$ and the backprojection operator $\mathcal{K}$, respectively. (The necessary notions from microlocal analysis are given in appendix A.) Thereafter, we use various criteria to choose the filter Q and analyse the singularities and statistics of the resulting target image $\hat{T}$.

3.1. Backprojection operator and the analysis of the singularities of image statistics

We use the following notation for the first- and second-order statistics of the image:

$$\hat{\mu}(z) := E[\hat{T}(z)], \tag{12}$$

$$\mathcal{C}_{\mathcal{K}n}(z, z') := E[\mathcal{K}n(z)\overline{\mathcal{K}n(z')}], \tag{13}$$

$$\mathcal{C}_{\hat{T}}(z, z') := E[(\hat{T}(z) - \hat{\mu}(z))\overline{(\hat{T}(z') - \hat{\mu}(z'))}]. \tag{14}$$

The following theorem states how the singularities of the first- and second-order statistics of the scene are related to those of the reconstructed image.

Theorem 1. *We assume that the image $\hat{T}$ is formed via (10), where Q satisfies a symbol estimate and where the data d are given by (3). We assume that the geometrical conditions on the flight trajectory and antenna beam pattern outlined in [9] for avoiding artefacts are satisfied. Then the singularities of the first- and second-order statistics of $\hat{T}$ have the properties*

(i) $\mathrm{WF}(\hat{\mu}) \subseteq \mathrm{WF}(\mu)$,
(ii) $\mathrm{WF}(\mathcal{C}_{\hat{T}}) \subseteq \mathrm{WF}(\mathcal{C}_T + \mathcal{R}_C) \cup \mathrm{WF}(\mathcal{C}_{\mathcal{K}n})$,

where WF *denotes the wavefront set (see appendix A) and where $\mathcal{C}_T$, $\mathcal{R}_C$ are given by (7) and (8), respectively.*

Conclusion (i) tells us that the singularities appearing in the first-order image statistics are correctly located. Conclusion (ii) tells us that corresponding relationship for the second-order statistics can be more complicated: it is possible for the clutter to contribute more singularities or for the clutter to cancel some of the singularities of the target autocovariance. Moreover, additional singularities due to noise may appear in the second-order statistics.

Proof. (i) *Singularities of the first-order statistics of the image* $\hat{T}$.
From (10) and (12)

$$\hat{\mu}(\boldsymbol{z}) = \mathcal{K}\mathcal{F}E[T(\boldsymbol{z})] = \mathcal{K}\mathcal{F}\mu(\boldsymbol{z}). \tag{15}$$

We simplify the product $\mathcal{K}\mathcal{F}$ to compute $\hat{\mu}$. Using (1) in (10) and carrying out the t integration and one of the ω integrations results in

$$\mathcal{K}\mathcal{F}\mu(\boldsymbol{z}) = \int \mathrm{e}^{\mathrm{i}2\pi(2\omega/c)(|\mathbf{r}_{s,\boldsymbol{x}}|-|\mathbf{r}_{s,\boldsymbol{z}}|)} Q(\boldsymbol{z}, s, \omega) A(\boldsymbol{x}, s, \omega)\mu(\boldsymbol{x})\, \mathrm{d}\omega\, \mathrm{d}s\, \mathrm{d}\boldsymbol{x}. \tag{16}$$

As in [9], we use the identity

$$h(\boldsymbol{x}) - h(\boldsymbol{z}) = (\boldsymbol{x} - \boldsymbol{z}) \cdot \int_0^1 \nabla h(\boldsymbol{z} + \lambda(\boldsymbol{x} - \boldsymbol{z}))\, \mathrm{d}\lambda \tag{17}$$

with $h(\boldsymbol{x}) = (2\omega/c)|\mathbf{r}_{s,\boldsymbol{x}}|$ to write the exponent of (16) as

$$\frac{2\omega}{c}(|\mathbf{r}_{s,\boldsymbol{x}}| - |\mathbf{r}_{s,\boldsymbol{z}}|) = \frac{2\omega}{c}(\boldsymbol{x} - \boldsymbol{z}) \cdot \boldsymbol{\Xi}(s, \boldsymbol{x}, \boldsymbol{z}), \tag{18}$$

where, for $\boldsymbol{x} = \boldsymbol{z}$,

$$\boldsymbol{\Xi}(s, \boldsymbol{z}, \boldsymbol{z}) = \nabla h(\boldsymbol{z}) = \widehat{\mathbf{r}_{s,\boldsymbol{z}}} \cdot D\boldsymbol{\psi}(\boldsymbol{z}) \tag{19}$$

and D denotes the derivative with respect to $\boldsymbol{z}$. Our assumption about the geometrical conditions on the flight trajectory and antenna beam pattern implies that the leading order contributions to (16) (from the method of stationary phase) come from the single critical point $\boldsymbol{x} = \boldsymbol{z}$. In the inner integral of (16) (i.e., for each $\boldsymbol{x}$ and $\boldsymbol{z}$), we then make the (Stolt) change of variables

$$(s, \omega) \to \boldsymbol{\xi} = \frac{2\omega}{c}\boldsymbol{\Xi}(s, \boldsymbol{x}, \boldsymbol{z}). \tag{20}$$

Again, the geometrical assumptions ensure that this change of variables is nonsingular. The change of variables (20) transforms the integral (16) into

$$\mathcal{K}\mathcal{F}\mu(\boldsymbol{z}) = \int \mathrm{e}^{\mathrm{i}2\pi(\boldsymbol{x}-\boldsymbol{z})\cdot\boldsymbol{\xi}} Q(\boldsymbol{z}, \boldsymbol{\xi}) A(\boldsymbol{x}, \boldsymbol{\xi}) \eta(\boldsymbol{x}, \boldsymbol{z}, \boldsymbol{\xi}) \mu(\boldsymbol{x})\, \mathrm{d}\boldsymbol{\xi}\, \mathrm{d}\boldsymbol{x}, \tag{21}$$

where $A(\boldsymbol{x}, \boldsymbol{\xi}) = A(\boldsymbol{x}, s(\boldsymbol{\xi}), \omega(\boldsymbol{\xi}))$, etc, and where

$$\eta(\boldsymbol{x}, \boldsymbol{z}, \boldsymbol{\xi}) = |\partial(s, \omega)/\partial\boldsymbol{\xi}| \tag{22}$$

is the Jacobian that comes from the change of variables (20).

Equation (21) exhibits the operator $\mathcal{K}\mathcal{F}$ as a pseudodifferential operator; and because pseudodifferential operators are pseudolocal (see appendix A), we have conclusion (i).

(ii) *Singularities of the second-order statistics of the image* $\hat{T}$.

The autocovariance of the image is

$$\begin{aligned} \mathcal{C}_{\hat{T}}(\boldsymbol{z}, \boldsymbol{z}') &= E[(\hat{T}(\boldsymbol{z}) - \hat{\mu}(\boldsymbol{z}))\overline{(\hat{T}(\boldsymbol{z}') - \hat{\mu}(\boldsymbol{z}'))}] \\ &= E[\mathcal{K}\mathcal{F}(T(\boldsymbol{z}) - \mu(\boldsymbol{z}))\overline{\mathcal{K}\mathcal{F}(T(\boldsymbol{z}') - \mu(\boldsymbol{z}'))}] \\ &\quad + E[\mathcal{K}\mathcal{F}C(\boldsymbol{z})\overline{\mathcal{K}\mathcal{F}C(\boldsymbol{z}')}] + E[\mathcal{K}n(\boldsymbol{z})\overline{\mathcal{K}n(\boldsymbol{z}')}], \end{aligned} \tag{23}$$

where the cross terms vanish because the target, clutter and noise are mutually statistically independent. The target and clutter terms can be treated together; the autocovariance of the sum we denote by $\mathcal{C}_{\mathcal{KF}(T+C)}$:

$$\begin{aligned}\mathcal{C}_{\mathcal{KF}(T+C)}(\boldsymbol{z},\boldsymbol{z}') &= E[\mathcal{KF}(T(\boldsymbol{z})-\mu(\boldsymbol{z}))\overline{\mathcal{KF}(T(\boldsymbol{z}')-\mu(\boldsymbol{z}'))}] + E[\mathcal{KF}C(\boldsymbol{z})\overline{\mathcal{KF}C(\boldsymbol{z}')}] \\ &= \int \mathrm{e}^{\mathrm{i}2\pi(2\omega/c)(|\mathbf{r}_{s,\boldsymbol{x}}|-|\mathbf{r}_{s,z}|)}\,Q(\boldsymbol{z},s,\omega)A(\boldsymbol{x},s,\omega)[\mathcal{C}_T(\boldsymbol{x},\boldsymbol{x}')+\mathcal{R}_C(\boldsymbol{x},\boldsymbol{x}')]\,\mathrm{d}\omega\,\mathrm{d}s\,\mathrm{d}\boldsymbol{x} \\ &\quad\times\int \mathrm{e}^{-\mathrm{i}2\pi(2\omega'/c)(|\mathbf{r}_{s',\boldsymbol{x}'}|-|\mathbf{r}_{s',z'}|)}\overline{Q(\boldsymbol{z}',s',\omega')A(\boldsymbol{x}',s',\omega')}\,\mathrm{d}\omega'\,\mathrm{d}s'\,\mathrm{d}\boldsymbol{x}'. \end{aligned} \tag{24}$$

We again use identity (17), this time with $h(\boldsymbol{x},\boldsymbol{x}') = |\mathbf{r}_{s,\boldsymbol{x}}| + |\mathbf{r}_{s',\boldsymbol{x}'}|$, and make the change of variables $(s,\omega)\mapsto\boldsymbol{\xi}$ and $(s',\omega')\mapsto\boldsymbol{\xi}'$ to obtain

$$\begin{aligned}\mathcal{C}_{\mathcal{KF}(T+C)}(\boldsymbol{z},\boldsymbol{z}') &= \int \mathrm{e}^{\mathrm{i}2\pi((\boldsymbol{x},\boldsymbol{x}')-(\boldsymbol{z},\boldsymbol{z}'))\cdot(\boldsymbol{\xi},\boldsymbol{\xi}')}\,Q(\boldsymbol{x},\boldsymbol{\xi})A(\boldsymbol{x},\boldsymbol{\xi})\eta(\boldsymbol{x},\boldsymbol{z},\boldsymbol{\xi})\,\mathrm{d}\boldsymbol{\xi}\,\mathrm{d}\boldsymbol{x} \\ &\quad\times[\mathcal{C}_T(\boldsymbol{x},\boldsymbol{x}')+\mathcal{R}_C(\boldsymbol{x},\boldsymbol{x}')]\overline{Q(\boldsymbol{x}',\boldsymbol{\xi}')A(\boldsymbol{x}',\boldsymbol{\xi}')}\eta(\boldsymbol{x}',\boldsymbol{z}',\boldsymbol{\xi}')\,\mathrm{d}\boldsymbol{\xi}'\,\mathrm{d}\boldsymbol{x}'. \end{aligned} \tag{25}$$

The same argument as in (i) above results in conclusion (ii). □

To see that noise can contribute to singularities of the second-order statistics, we consider the following example. First we compute $\mathcal{C}_{\mathcal{K}n}$:

$$\begin{aligned}\mathcal{C}_{\mathcal{K}n}(\boldsymbol{z},\boldsymbol{z}') &= \int \mathrm{e}^{\mathrm{i}2\pi\omega(t-2|\mathbf{r}_{s,z}|/c)}\,Q(\boldsymbol{z},s,\omega)\mathcal{R}_n(s,t,s',t') \\ &\quad\times \mathrm{e}^{-\mathrm{i}2\pi\omega'(t'-2|\mathbf{r}_{s',z'}|/c)}\overline{Q(\boldsymbol{z}',s,\omega)}\,\mathrm{d}\omega\,\mathrm{d}\omega'\,\mathrm{d}s\,\mathrm{d}t\,\mathrm{d}s'\,\mathrm{d}t'. \end{aligned} \tag{26}$$

We now assume that the noise is stationary in the fast time variable t and statistically uncorrelated in the slow time variable s, so that

$$\mathcal{R}_n(s,t;s',t') = \tilde{\mathcal{R}}_n(t-t',s)\delta(s-s'). \tag{27}$$

The dependence of $\tilde{\mathcal{R}}_n$ on s indicates that the noise is stationary, but not necessarily identically distributed in the slow time variable s. We denote the power spectral density function of $n(s,t)$ by S_n

$$\tilde{\mathcal{R}}_n(\tau,s) = \int \mathrm{e}^{-\mathrm{i}2\pi\omega\tau}\,S_n(\omega,s)\,\mathrm{d}\omega \tag{28}$$

for each fixed slow time variable s. If we use (27) and (28) in the first line of (26) and carry out the integrations over t, t', s' and ω', we obtain

$$\mathcal{C}_{\mathcal{K}n}(\boldsymbol{z},\boldsymbol{z}') = \int \mathrm{e}^{\mathrm{i}2\pi(2\omega/c)(|\mathbf{r}_{s,z'}|-|\mathbf{r}_{s,z}|)}\,Q(\boldsymbol{z},s,\omega)\overline{Q(\boldsymbol{z}',s,\omega)}S_n(\omega,s)\,\mathrm{d}\omega\,\mathrm{d}s. \tag{29}$$

In (29), we apply the same change of variables as in theorem 1, but with $\boldsymbol{x}$ replaced by $\boldsymbol{z}'$. This transforms (29) to

$$\mathcal{C}_{\mathcal{K}n}(\boldsymbol{z},\boldsymbol{z}') = \int \mathrm{e}^{\mathrm{i}2\pi(\boldsymbol{z}'-\boldsymbol{z})\cdot\boldsymbol{\xi}}\,Q(\boldsymbol{z},\boldsymbol{\xi})\overline{Q(\boldsymbol{z}',\boldsymbol{\xi})}S_n(\boldsymbol{\xi})\eta(\boldsymbol{z}',\boldsymbol{z},\boldsymbol{\xi})\,\mathrm{d}\boldsymbol{\xi}, \tag{30}$$

whose singularities are determined by the large-$\boldsymbol{\xi}$ decay of $Q(\boldsymbol{z},\boldsymbol{\xi})\overline{Q(\boldsymbol{z}',\boldsymbol{\xi})}S_n(\boldsymbol{\xi})\eta(\boldsymbol{z}',\boldsymbol{z},\boldsymbol{\xi})$. If the noise power spectral density decays slowly for large $\boldsymbol{\xi}$, then $\mathcal{C}_{\mathcal{K}n}(\boldsymbol{z},\boldsymbol{z}')$ will have singularities at $\boldsymbol{z}=\boldsymbol{z}'$.

3.2. Determination of the filter Q

The analysis above shows that the backprojection operator puts the singularities of the first- and second-order statistics of the target scene T at the right location and orientation in the reconstructed target image $\hat{T}$, even if the filter Q is chosen as the unity filter. Not all singularities in the scene will appear in the image; a singularity is *visible* at a point z in the image if its wavefront set contains the direction $\widehat{r_{s,z}}$ and $A(z, s, \omega) \neq 0$ for some ω [8, 9, 18].

The analysis above shows that the second-order statistics of $\hat{T}$ may contain additional singularities due to noise and clutter. However, we show below that the filter Q can be determined so that either

(1) the visible singularities of the first-order statistics of the reconstructed target image $\hat{T}$ have not only the correct location and orientation but also the *correct strengths*, i.e., the bias of the estimator is one degree smoother than the image itself, or
(2) the strength of the singularities of the second-order statistics of clutter and noise can be suppressed so that the mean-square error between the target scene and image is minimized.

In other words, there is a trade-off between bias and variance: a minimum-variance estimate is biased.

Below, we will determine the filter Q based on these two different criteria and analyse the properties of the resulting estimators.

(1) *Determination of Q to preserve the strength of singularities of the first-order statistics.*

Given our flight trajectory and bandwidth, the best possible image (in the least-squares sense) we could construct would be

$$T_\Omega(z) := \int_{\Omega_z} \mathrm{e}^{\mathrm{i}2\pi(z'-z)\cdot\xi} T(z')\,\mathrm{d}\xi\,\mathrm{d}z', \tag{31}$$

where Ω_z is the data collection manifold given by

$$\Omega_z = \{\xi = 2(\omega/c)\widehat{\mathbf{r}_{s,z}} \cdot D\psi(z) : A(z, s, \omega) \text{ is nonzero}\}. \tag{32}$$

The image T_Ω, however, will exhibit undesirable ringing because the integral (31) involves a sharp characteristic function χ_Ω. To avoid the ringing, we could approximate χ_Ω by a smoothed $\tilde{\chi}_\Omega$, which is 0 outside the set Ω_z and 1 in most of the interior. The corresponding image is

$$T_{\tilde{\chi}}(z) = \mathcal{I}_\Omega T(z) := \int \tilde{\chi}_\Omega(z, \xi)\,\mathrm{e}^{\mathrm{i}2\pi(z'-z)\cdot\xi} T(z')\,\mathrm{d}\xi\,\mathrm{d}z'. \tag{33}$$

To avoid introducing new notation, for the rest of the paper, we drop the subscript $\tilde{\chi}$ and write simply T. (Thus without loss of generality, we assume below that all singularities are visible.)

Let $B(Q)$ be the bias of the estimator defined by

$$B(Q)(z) := E[\hat{T}(z)] - E[T(z)]. \tag{34}$$

The theorem below states that Q can be chosen so that the estimate is unbiased to leading order, in the sense that it is smoother than the mean. However, this estimate has the undesirable property of preserving the strength of the clutter singularities in the second-order statistics of the image.

Theorem 2. *Let $d(s, t)$ be given by (3) and $\hat{T}(z)$ be given by (10). If the filter Q in (10) is chosen as*

$$Q(z, s, \omega) = \frac{\tilde{\chi}_\Omega(z, s, \omega)}{A(z, s, \omega)\eta(z, z, s, \omega)}, \tag{35}$$

where $\eta(z, z, s, \omega)$ is as defined in equations (20) and (22), and $\tilde{\chi}_\Omega$ is the smooth cut-off function defined above (33), then

(i) the bias of the estimator $B(Q)$ is one degree smoother than $E[\hat{T}(\boldsymbol{z})]$;
(ii) $\mathcal{C}_{\mathcal{KF}(T+C)}(\boldsymbol{z},\boldsymbol{z}') - [\mathcal{C}_T(\boldsymbol{z},\boldsymbol{z}') + \mathcal{R}_C(\boldsymbol{z},\boldsymbol{z}')]$ is one degree smoother than $\mathcal{C}_{\mathcal{KF}(T+C)}$, where $\mathcal{C}_T$ and $\mathcal{R}_C$ are given by (7) and (8), respectively;
(iii) if the noise satisfies (27), the autocovariance function $\mathcal{C}_{\mathcal{K}n}$ may have singularities at $\boldsymbol{z}=\boldsymbol{z}'$, depending on the large-$\boldsymbol{\xi}$ decay of $S_n(\boldsymbol{\xi})$, where S_n is defined by (28).

Proof. (i) *First-order statistics.* Note that the bias of the estimator is

$$B(Q)(\boldsymbol{z}) = (\mathcal{KF} - \mathcal{I}_\Omega)\mu(\boldsymbol{z}). \tag{36}$$

Our objective is to determine Q so that the estimate is unbiased, at least to leading order; in other words, we want $\mathcal{KF} \approx \mathcal{I}_\Omega$. Since the leading order term of (21) comes from $\boldsymbol{z}=\boldsymbol{x}$, this is equivalent to setting

$$Q(\boldsymbol{z},\boldsymbol{\xi})A(\boldsymbol{x},\boldsymbol{\xi})\eta(\boldsymbol{x},\boldsymbol{z},\boldsymbol{\xi}) = \tilde{\chi}_\Omega(\boldsymbol{z},\boldsymbol{\xi}) \tag{37}$$

which leads to the filter (35) where $\eta(\boldsymbol{z},\boldsymbol{z},\boldsymbol{\xi})$ is as defined in equations (22) and (20).

We note that Q satisfies a symbol estimate [10–12]; moreover, the filter (35) is the same as the filter given in [8, 9]. This filter gives us images $\hat{T}$ whose first-order statistics show the visible singularities at the correct location, orientation and strength.

(ii) *Target and clutter component of image autocovariance.* With the choice of filter (35), from (25), the target and clutter terms of the image autocovariance (14) become

$$\begin{aligned}\mathcal{C}_{\mathcal{KF}(T+C)}(\boldsymbol{z},\boldsymbol{z}') = \int \mathrm{e}^{\mathrm{i}2\pi((\boldsymbol{x},\boldsymbol{x}')-(\boldsymbol{z},\boldsymbol{z}'))\cdot(\boldsymbol{\xi},\boldsymbol{\xi}')} \frac{\tilde{\chi}_\Omega(\boldsymbol{z},\boldsymbol{\xi})A(\boldsymbol{x},\boldsymbol{\xi})\eta(\boldsymbol{x},\boldsymbol{z},\boldsymbol{\xi})}{A(\boldsymbol{z},\boldsymbol{\xi})\eta(\boldsymbol{z},\boldsymbol{z},\boldsymbol{\xi})} \\ \times \frac{\tilde{\chi}_\Omega(\boldsymbol{z}',\boldsymbol{\xi}')\overline{A(\boldsymbol{x}',\boldsymbol{\xi}')}\eta(\boldsymbol{x}',\boldsymbol{z}',\boldsymbol{\xi}')}{\overline{A(\boldsymbol{z}',\boldsymbol{\xi}')}\eta(\boldsymbol{z}',\boldsymbol{z}',\boldsymbol{\xi}')}\,\mathrm{d}\boldsymbol{\xi}\,\mathrm{d}\boldsymbol{\xi}'[\mathcal{C}_T(\boldsymbol{x},\boldsymbol{x}') + \mathcal{R}_C(\boldsymbol{x},\boldsymbol{x}')]\,\mathrm{d}\boldsymbol{x}\,\mathrm{d}\boldsymbol{x}',\end{aligned} \tag{38}$$

where we have used the fact that the cut-off $\tilde{\chi}_\Omega$ and Jacobian η are real. The leading order contribution to (38) occurs when $\boldsymbol{z}=\boldsymbol{x}$ and $\boldsymbol{z}'=\boldsymbol{x}'$, which implies that to leading order

$$\mathcal{C}_{\mathcal{KF}(T+C)}(\boldsymbol{z},\boldsymbol{z}') \sim \int_{\Omega_z}\int_{\Omega_{z'}} \mathrm{e}^{\mathrm{i}2\pi((\boldsymbol{x},\boldsymbol{x}')-(\boldsymbol{z},\boldsymbol{z}'))\cdot(\boldsymbol{\xi},\boldsymbol{\xi}')}[\mathcal{C}_T(\boldsymbol{x},\boldsymbol{x}') + \mathcal{R}_C(\boldsymbol{x},\boldsymbol{x}')]\,\mathrm{d}\boldsymbol{\xi}\,\mathrm{d}\boldsymbol{\xi}'\mathrm{d}\boldsymbol{x}\,\mathrm{d}\boldsymbol{x}'. \tag{39}$$

We see that again the location and orientation of visible singularities of $\mathcal{C}_T(\boldsymbol{x},\boldsymbol{x}') + \mathcal{R}_C(\boldsymbol{x},\boldsymbol{x}')$ are preserved in $\mathcal{C}_{\mathcal{KF}(T+C)}(\boldsymbol{z},\boldsymbol{z}')$ and are of the same strength as $\mathcal{C}_T(\boldsymbol{x},\boldsymbol{x}') + \mathcal{R}_C(\boldsymbol{x},\boldsymbol{x}')$.

(iii) *Noise component of image autocovariance.* The noise term, on the other hand, from (30) is

$$\mathcal{C}_{\mathcal{K}n}(\boldsymbol{z},\boldsymbol{z}') = \int \mathrm{e}^{\mathrm{i}2\pi(\boldsymbol{z}'-\boldsymbol{z})\cdot\boldsymbol{\xi}} \frac{\tilde{\chi}_\Omega(\boldsymbol{z},\boldsymbol{\xi})}{A(\boldsymbol{z},\boldsymbol{\xi})} \frac{\tilde{\chi}_\Omega(\boldsymbol{z}',\boldsymbol{\xi})}{\overline{A(\boldsymbol{z}',\boldsymbol{\xi})}\eta(\boldsymbol{z}',\boldsymbol{z},\boldsymbol{\xi})} S_n(\boldsymbol{\xi})\,\mathrm{d}\boldsymbol{\xi}. \tag{40}$$

We see that, depending on the large-$\boldsymbol{\xi}$ decay of $S_n(\boldsymbol{\xi})$, singularities can appear at $\boldsymbol{z}=\boldsymbol{z}'$. □

(2) *Determination of Q so that noise and clutter strength is minimized.*

We now want to make a different choice for Q, namely one that suppresses the strength of the singularities of the second-order statistics of noise and clutter.

We define the following error process:

$$\mathcal{E}(\boldsymbol{z}) = \hat{T}(\boldsymbol{z}) - T(\boldsymbol{z}), \tag{41}$$

and the mean-square error as

$$\mathcal{J}(Q) = \int E[|\mathcal{E}(\boldsymbol{z})|^2]\,\mathrm{d}\boldsymbol{z}. \tag{42}$$

The mean-square error comprises two components:

$$\mathcal{J}(Q) = \mathcal{V}(Q) + \mathcal{B}(Q), \tag{43}$$

where $\mathcal{V}(Q)$ is the total variance of $\mathcal{E}(\boldsymbol{z})$ defined as

$$\mathcal{V}(Q) = \int E[|\mathcal{E}(\boldsymbol{z}) - E[\mathcal{E}(\boldsymbol{z})]|^2]\,\mathrm{d}\boldsymbol{z}, \tag{44}$$

and $\mathcal{B}(Q)$ is the square of the L^2-norm of the bias

$$\mathcal{B}(Q) = \int |B(Q)(\boldsymbol{z})|^2\,\mathrm{d}\boldsymbol{z}. \tag{45}$$

We will first determine the filter Q so that the mean-square error $\mathcal{J}(Q)$ is minimized. Next, we will make the assumption that the clutter and noise are stationary and that the target is stationary up to its mean, and derive an explicit formula for Q minimizing $\mathcal{V}(Q)$, the total variance of the error.

Theorem 3. *Let $d(s,t)$ be given by (3) and $\hat{T}(\boldsymbol{z})$ be given by (10). Assume that $\mathcal{R}_n(s,t;s',t')$ is given by (27), $\tilde{S}_n = S_n/(2\pi)^4$ where S_n is given by (28), and define $\tilde{S}_T$ and $\tilde{S}_C$ by*

$$\mathcal{C}_T(\boldsymbol{x},\boldsymbol{x}') = \int \mathrm{e}^{-\mathrm{i}2\pi\boldsymbol{x}\cdot\boldsymbol{\zeta}}\,\mathrm{e}^{\mathrm{i}2\pi\boldsymbol{x}'\cdot\boldsymbol{\zeta}'}\,\tilde{S}_T(\boldsymbol{\zeta},\boldsymbol{\zeta}')\,\mathrm{d}\boldsymbol{\zeta}\,\mathrm{d}\boldsymbol{\zeta}', \tag{46}$$

$$\mathcal{R}_C(\boldsymbol{x},\boldsymbol{x}') = \int \mathrm{e}^{-\mathrm{i}2\pi\boldsymbol{x}\cdot\boldsymbol{\zeta}}\,\mathrm{e}^{\mathrm{i}2\pi\boldsymbol{x}'\cdot\boldsymbol{\zeta}'}\,\tilde{S}_C(\boldsymbol{\zeta},\boldsymbol{\zeta}')\,\mathrm{d}\boldsymbol{\zeta}\,\mathrm{d}\boldsymbol{\zeta}'. \tag{47}$$

(i) Then any filter Q satisfying a symbol estimate and also minimizing the mean-square error $\mathcal{J}(Q)$ must be a solution of the following integral equation:

$$\int \overline{A}\eta(\mathrm{e}^{\mathrm{i}2\pi\boldsymbol{x}\cdot(\boldsymbol{\zeta}-\boldsymbol{\zeta}')}QA\eta(\tilde{S}_T + M\overline{M'} + \tilde{S}_C) - (\tilde{S}_T + M\overline{M'})\tilde{\chi}_\Omega)\,\mathrm{d}\boldsymbol{\zeta}' + \tilde{S}_n Q\eta = 0, \tag{48}$$

where $M = M(\zeta)$ is the Fourier transform of μ, $M' = M(\zeta')$, $\eta = \eta(\boldsymbol{x},\boldsymbol{x},\boldsymbol{\zeta})$ is as defined in (22) and $\tilde{\chi}_\Omega(\boldsymbol{x},\boldsymbol{\zeta})$ is defined above (33).

(ii) Assume that clutter is stationary, i.e.,

$$E[C(\boldsymbol{x})\overline{C(\boldsymbol{x}')}] = \tilde{R}_C(\boldsymbol{x}-\boldsymbol{x}'). \tag{49}$$

Assume also that the target is stationary up to its mean:

$$E[(T(\boldsymbol{x}) - \mu(\boldsymbol{x}))\overline{(T(\boldsymbol{x}') - \mu(\boldsymbol{x}'))}] = \tilde{C}_T(\boldsymbol{x}-\boldsymbol{x}'). \tag{50}$$

Note that $\tilde{R}_C$ and $\tilde{C}_T$ are even functions. Let S_T and S_C be the power spectral density functions of $T(\boldsymbol{x}) - \mu(\boldsymbol{x})$ and $C(\boldsymbol{x})$, respectively, i.e.,

$$\tilde{C}_T(\boldsymbol{y}) = \int \mathrm{e}^{\mathrm{i}2\pi\boldsymbol{y}\cdot\boldsymbol{\zeta}} S_T(\boldsymbol{\zeta})\,\mathrm{d}\boldsymbol{\zeta}, \tag{51}$$

$$\tilde{\mathcal{R}}_C(\boldsymbol{y}) = \int \mathrm{e}^{\mathrm{i}2\pi\boldsymbol{y}\cdot\boldsymbol{\zeta}} S_C(\boldsymbol{\zeta})\,\mathrm{d}\boldsymbol{\zeta}. \tag{52}$$

Assume that S_T, S_C and S_n are smooth and satisfy symbol estimates. Then the filter Q minimizing the total error variance $\mathcal{V}(Q)$ is given by

$$Q(\boldsymbol{x},\boldsymbol{\xi}) = \frac{\tilde{\chi}_\Omega(\boldsymbol{x},\boldsymbol{\xi})S_T(\boldsymbol{\xi})\overline{A(\boldsymbol{x},\boldsymbol{\xi})}}{|A(\boldsymbol{x},\boldsymbol{\xi})|^2\eta(\boldsymbol{x},\boldsymbol{\xi})[S_T(\boldsymbol{\xi}) + S_C(\boldsymbol{\xi})] + \tilde{S}_n(\boldsymbol{\xi})}. \tag{53}$$

Proof. (i) We want to determine Q so that the quantity

$$\mathcal{J}(Q) = \int E[|\mathcal{K}(\mathcal{F}[T+C]+n)(\boldsymbol{z}) - T(\boldsymbol{z})|^2]\,\mathrm{d}\boldsymbol{z} = \mathcal{J}_T(Q) + \mathcal{J}_C(Q) + \mathcal{J}_n(Q) \tag{54}$$

is minimized, where

$$\mathcal{J}_T(Q) = \int E[|(\mathcal{K}\mathcal{F} - \mathcal{I}_\Omega)T(\boldsymbol{z})|^2]\,\mathrm{d}\boldsymbol{z}, \tag{55}$$

$$\mathcal{J}_C(Q) = \int E[|\mathcal{K}\mathcal{F}C(\boldsymbol{z})|^2]\,\mathrm{d}\boldsymbol{z}, \tag{56}$$

$$\mathcal{J}_n(Q) = \int E[|\mathcal{K}n(\boldsymbol{z})|^2]\,\mathrm{d}\boldsymbol{z}, \tag{57}$$

with $\mathcal{I}_\Omega$ as defined in (31). Again the cross terms of (54) disappear because we are assuming that the target, clutter and noise are all statistically independent.

We first simplify each of the expressions (55)–(57). In (55), we write $\mathcal{K}\mathcal{F}$ as in (21) and $\mathcal{I}_\Omega$ as in (31) to obtain

$$\begin{aligned}\mathcal{J}_T(Q) = \int \mathrm{e}^{\mathrm{i}2\pi(\boldsymbol{x}-\boldsymbol{z})\cdot\boldsymbol{\xi}}[Q(\boldsymbol{z},\boldsymbol{\xi})A(\boldsymbol{x},\boldsymbol{\xi})\eta(\boldsymbol{x},\boldsymbol{z},\boldsymbol{\xi}) - \tilde{\chi}_\Omega(\boldsymbol{z},\boldsymbol{\xi})](\mathcal{C}_T(\boldsymbol{x},\boldsymbol{x}') + \mu(\boldsymbol{x})\overline{\mu(\boldsymbol{x}')})\,\mathrm{d}\boldsymbol{\xi}\,\mathrm{d}\boldsymbol{x} \\ \times \int \mathrm{e}^{-\mathrm{i}2\pi(\boldsymbol{x}'-\boldsymbol{z}')\cdot\boldsymbol{\xi}'}\overline{[Q(\boldsymbol{z},\boldsymbol{\xi}')A(\boldsymbol{x}',\boldsymbol{\xi}')\eta(\boldsymbol{x}',\boldsymbol{z},\boldsymbol{\xi}') - \tilde{\chi}_\Omega(\boldsymbol{z},\boldsymbol{\xi}')]}\,\mathrm{d}\boldsymbol{\xi}'\,\mathrm{d}\boldsymbol{x}'\,\mathrm{d}\boldsymbol{z},\end{aligned} \tag{58}$$

where $\tilde{\chi}_\Omega(\boldsymbol{z},\boldsymbol{\zeta})$ denotes the characteristic function of the data collection manifold Ω_z defined in (32). We see that $\mathcal{J}_T$ splits into two terms:

$$\mathcal{J}_T(Q) = \tilde{\mathcal{J}}_T(Q) + \mathcal{B}(Q), \tag{59}$$

where $\tilde{\mathcal{J}}_T(Q)$ involves only $\mathcal{C}_T$ but not μ.

We apply the method of stationary phase to the $\boldsymbol{z}$ and $\boldsymbol{\xi}'$ integrals of (58). (The phase is $(\boldsymbol{x}-\boldsymbol{z})\cdot\boldsymbol{\xi} - (\boldsymbol{x}'-\boldsymbol{z})\cdot\boldsymbol{\xi}'$, so the critical conditions are $\boldsymbol{\xi} = \boldsymbol{\xi}'$ and $\boldsymbol{z} = \boldsymbol{x}'$.) The leading order contribution to (58) is the sum of the two terms

$$\begin{aligned}\tilde{\mathcal{J}}_T(Q) \sim \int \mathrm{e}^{\mathrm{i}2\pi(\boldsymbol{x}-\boldsymbol{x}')\cdot\boldsymbol{\xi}}[Q(\boldsymbol{x}',\boldsymbol{\xi})A(\boldsymbol{x},\boldsymbol{\xi})\eta(\boldsymbol{x},\boldsymbol{x}',\boldsymbol{\xi}) - \tilde{\chi}_\Omega(\boldsymbol{x}',\boldsymbol{\xi})] \\ \times \mathcal{C}_T(\boldsymbol{x},\boldsymbol{x}')\overline{[Q(\boldsymbol{x}',\boldsymbol{\xi})A(\boldsymbol{x}',\boldsymbol{\xi})\eta(\boldsymbol{x}',\boldsymbol{x}',\boldsymbol{\xi}) - \tilde{\chi}_\Omega(\boldsymbol{x}',\boldsymbol{\xi})]}\,\mathrm{d}\boldsymbol{\xi}\,\mathrm{d}\boldsymbol{x}\,\mathrm{d}\boldsymbol{x}',\end{aligned} \tag{60}$$

and

$$\begin{aligned}\mathcal{B}(Q) \sim \int \mathrm{e}^{\mathrm{i}2\pi(\boldsymbol{x}-\boldsymbol{x}')\cdot\boldsymbol{\xi}}[Q(\boldsymbol{x}',\boldsymbol{\xi})A(\boldsymbol{x},\boldsymbol{\xi})\eta(\boldsymbol{x},\boldsymbol{x}',\boldsymbol{\xi}) - \tilde{\chi}_\Omega(\boldsymbol{x}',\boldsymbol{\xi})] \\ \times \mu(\boldsymbol{x})\overline{\mu(\boldsymbol{x}')[Q(\boldsymbol{x}',\boldsymbol{\xi})A(\boldsymbol{x}',\boldsymbol{\xi})\eta(\boldsymbol{x}',\boldsymbol{x}',\boldsymbol{\xi}) - \tilde{\chi}_\Omega(\boldsymbol{x}',\boldsymbol{\xi})]}\,\mathrm{d}\boldsymbol{\xi}\,\mathrm{d}\boldsymbol{x}\,\mathrm{d}\boldsymbol{x}'.\end{aligned} \tag{61}$$

To $\mathcal{J}_C$ we apply the same procedures, i.e., write $\mathcal{K}\mathcal{F}$ as in (21) and apply the stationary phase theorem. This results in the leading order term:

$$\begin{aligned}\mathcal{J}_C(Q) \sim \int \mathrm{e}^{\mathrm{i}2\pi(\boldsymbol{x}-\boldsymbol{x}')\cdot\boldsymbol{\xi}}[Q(\boldsymbol{x}',\boldsymbol{\xi})A(\boldsymbol{x},\boldsymbol{\xi})\eta(\boldsymbol{x},\boldsymbol{x}',\boldsymbol{\xi})]\mathcal{R}_C(\boldsymbol{x},\boldsymbol{x}') \\ \times \overline{[Q(\boldsymbol{x}',\boldsymbol{\xi})A(\boldsymbol{x}',\boldsymbol{\xi})\eta(\boldsymbol{x}',\boldsymbol{x}',\boldsymbol{\xi})]}\,\mathrm{d}\boldsymbol{\xi}\,\mathrm{d}\boldsymbol{x}\,\mathrm{d}\boldsymbol{x}'.\end{aligned} \tag{62}$$

In the term $\mathcal{J}_n$, we use assumption (27) and definition (28), and using (30) we obtain

$$\mathcal{J}_n(Q) \sim \int |Q(\boldsymbol{z},\boldsymbol{\xi})|^2\tilde{S}_n(\boldsymbol{\xi})\eta(\boldsymbol{z},\boldsymbol{z},\boldsymbol{\xi})\,\mathrm{d}\boldsymbol{\xi}\,\mathrm{d}\boldsymbol{z}, \tag{63}$$

where in the last step we have made the change of variables (20).

We use (46) and (47) in (59) and (62) and then apply the method of stationary phase in the variables $\boldsymbol{x}$ and $\boldsymbol{\xi}$. (The phase is $(\boldsymbol{x}' - \boldsymbol{x}) \cdot \boldsymbol{\xi} + \boldsymbol{x} \cdot \boldsymbol{\zeta} - \boldsymbol{x}' \cdot \boldsymbol{\zeta}'$, so the critical conditions are $\boldsymbol{\xi} = \boldsymbol{\zeta}$ and $\boldsymbol{x}' = \boldsymbol{x}$.) The leading order term of (60) is then

$$\tilde{\mathcal{J}}_T(Q) \sim \int \mathrm{e}^{\mathrm{i}2\pi \boldsymbol{x}' \cdot (\boldsymbol{\zeta}' - \boldsymbol{\zeta})} |Q(\boldsymbol{x}', \boldsymbol{\zeta}) A(\boldsymbol{x}', \boldsymbol{\zeta}) \eta(\boldsymbol{x}', \boldsymbol{x}', \boldsymbol{\zeta}) - \tilde{\chi}_\Omega(\boldsymbol{x}', \boldsymbol{\zeta})|^2 \tilde{S}_T(\boldsymbol{\zeta}, \boldsymbol{\zeta}') \, \mathrm{d}\boldsymbol{\zeta} \, \mathrm{d}\boldsymbol{\zeta}' \, \mathrm{d}\boldsymbol{x}'. \tag{64}$$

Similarly, the leading order term of (62) is

$$\mathcal{J}_C(Q) \sim \int \mathrm{e}^{\mathrm{i}2\pi \boldsymbol{x}' \cdot (\boldsymbol{\zeta}' - \boldsymbol{\zeta})} |Q(\boldsymbol{x}', \boldsymbol{\zeta}) A(\boldsymbol{x}', \boldsymbol{\zeta}) \eta(\boldsymbol{x}', \boldsymbol{x}', \boldsymbol{\zeta})|^2 \tilde{S}_C(\boldsymbol{\zeta}, \boldsymbol{\zeta}') \, \mathrm{d}\boldsymbol{\zeta} \, \mathrm{d}\boldsymbol{\zeta}' \, \mathrm{d}\boldsymbol{x}'. \tag{65}$$

In (61), we write

$$\mu(\boldsymbol{x}) = \int \mathrm{e}^{-\mathrm{i}2\pi \boldsymbol{x} \cdot \boldsymbol{\zeta}} M(\boldsymbol{\zeta}) \, \mathrm{d}\boldsymbol{\zeta} \qquad \overline{\mu(\boldsymbol{x}')} = \int \mathrm{e}^{\mathrm{i}2\pi \boldsymbol{x}' \cdot \boldsymbol{\zeta}} \overline{M(\boldsymbol{\zeta})} \, \mathrm{d}\boldsymbol{\zeta}, \tag{66}$$

and carry out the same stationary phase calculation as above (64). This results in the leading order term

$$\mathcal{B}(Q) \sim \int \mathrm{e}^{\mathrm{i}\boldsymbol{x}' \cdot (\boldsymbol{\zeta}' - \boldsymbol{\zeta})} |Q(\boldsymbol{x}', \boldsymbol{\zeta}) A(\boldsymbol{x}', \boldsymbol{\zeta}) \eta(\boldsymbol{x}', \boldsymbol{x}', \boldsymbol{\zeta}) - \tilde{\chi}_\Omega(\boldsymbol{x}', \boldsymbol{\zeta})|^2 M(\boldsymbol{\zeta}) \overline{M(\boldsymbol{\zeta}')} \, \mathrm{d}\boldsymbol{\zeta} \, \mathrm{d}\boldsymbol{\zeta}' \, \mathrm{d}\boldsymbol{x}'. \tag{67}$$

We drop the primes on the dummy variable $\boldsymbol{x}'$ and write M' for $M(\boldsymbol{\zeta}')$.

Having obtained a simple form for (54), we find the filter Q for which (54) is minimized. To do this, we calculate the variation of $\mathcal{J}$ with respect to Q:

$$\begin{aligned} 0 = \frac{\mathrm{d}}{\mathrm{d}\epsilon}\bigg|_{\epsilon=0} \tilde{\mathcal{J}}_T(Q + \epsilon Q_\epsilon) + \frac{\mathrm{d}}{\mathrm{d}\epsilon}\bigg|_{\epsilon=0} \mathcal{J}_C(Q + \epsilon Q_\epsilon) \\ + \frac{\mathrm{d}}{\mathrm{d}\epsilon}\bigg|_{\epsilon=0} \mathcal{J}_n(Q + \epsilon Q_\epsilon) + \frac{\mathrm{d}}{\mathrm{d}\epsilon}\bigg|_{\epsilon=0} \mathcal{B}(Q + \epsilon Q_\epsilon). \end{aligned} \tag{68}$$

The first term on the right-hand side of (68) is, from (64),

$$\begin{aligned} \frac{\mathrm{d}}{\mathrm{d}\epsilon}\bigg|_{\epsilon=0} \tilde{\mathcal{J}}_T(Q + \epsilon Q_\epsilon) \sim \int \mathrm{e}^{\mathrm{i}2\pi \boldsymbol{x} \cdot (\boldsymbol{\zeta}' - \boldsymbol{\zeta})} Q_\epsilon A \eta \tilde{S}_T \overline{(QA\eta - \tilde{\chi})} \, \mathrm{d}\boldsymbol{\zeta} \, \mathrm{d}\boldsymbol{\zeta}' \, \mathrm{d}\boldsymbol{x} \\ + \int \mathrm{e}^{\mathrm{i}2\pi \boldsymbol{x} \cdot (\boldsymbol{\zeta}' - \boldsymbol{\zeta})} (QA\eta - \tilde{\chi}) \tilde{S}_T \overline{Q_\epsilon A \eta} \, \mathrm{d}\boldsymbol{\zeta} \, \mathrm{d}\boldsymbol{\zeta}' \, \mathrm{d}\boldsymbol{x}. \end{aligned} \tag{69}$$

Interchanging $\boldsymbol{\zeta}$ and $\boldsymbol{\zeta}'$ in the second integral of (69) and using the fact that $\overline{\tilde{S}_T(\boldsymbol{\zeta}, \boldsymbol{\zeta}')} = \tilde{S}_T(\boldsymbol{\zeta}', \boldsymbol{\zeta})$, we obtain

$$\frac{\mathrm{d}}{\mathrm{d}\epsilon}\bigg|_{\epsilon=0} \tilde{\mathcal{J}}_T(Q + \epsilon Q_\epsilon) \sim 2 \operatorname{Re} \int \mathrm{e}^{\mathrm{i}2\pi \boldsymbol{x} \cdot (\boldsymbol{\zeta}' - \boldsymbol{\zeta})} \overline{Q_\epsilon A \eta} \tilde{S}_T (QA\eta - \tilde{\chi}) \, \mathrm{d}\boldsymbol{\zeta} \, \mathrm{d}\boldsymbol{\zeta}' \, \mathrm{d}\boldsymbol{x}. \tag{70}$$

Similarly,

$$\frac{\mathrm{d}}{\mathrm{d}\epsilon}\bigg|_{\epsilon=0} \mathcal{J}_C(Q + \epsilon Q_\epsilon) \sim 2 \operatorname{Re} \int \mathrm{e}^{\mathrm{i}2\pi \boldsymbol{x} \cdot (\boldsymbol{\zeta}' - \boldsymbol{\zeta})} \overline{Q_\epsilon A \eta} \tilde{S}_C (QA\eta) \, \mathrm{d}\boldsymbol{\zeta} \, \mathrm{d}\boldsymbol{\zeta}' \, \mathrm{d}\boldsymbol{x}, \tag{71}$$

$$\frac{\mathrm{d}}{\mathrm{d}\epsilon}\bigg|_{\epsilon=0} \mathcal{J}_n(Q + \epsilon Q_\epsilon) \sim 2 \operatorname{Re} \int \tilde{S}_n(\overline{Q_\epsilon} Q) \eta \, \mathrm{d}\boldsymbol{\zeta} \, \mathrm{d}\boldsymbol{z}, \tag{72}$$

and

$$\frac{\mathrm{d}}{\mathrm{d}\epsilon}\bigg|_{\epsilon=0} \mathcal{B}(Q + \epsilon Q_\epsilon) \sim 2 \operatorname{Re} \int \mathrm{e}^{\mathrm{i}2\pi \boldsymbol{x} \cdot (\boldsymbol{\zeta}' - \boldsymbol{\zeta})} \overline{Q_\epsilon A \eta} M \overline{M'} (QA\eta - \tilde{\chi}) \, \mathrm{d}\boldsymbol{\zeta} \, \mathrm{d}\boldsymbol{\zeta}' \, \mathrm{d}\boldsymbol{x}. \tag{73}$$

Using expressions (70)–(73) in (68), we obtain

$$0 \sim 2\,\mathrm{Re}\int \overline{Q_\epsilon}\Big(\int \overline{A}\eta\, \mathrm{e}^{\mathrm{i}2\pi \boldsymbol{x}\cdot(\zeta'-\zeta)}(QA\eta(\tilde{S}_T + M\overline{M'} + \tilde{S}_C) - (\tilde{S}_T + M\overline{M'})\tilde{\chi})\,\mathrm{d}\zeta' + \tilde{S}_n Q\eta\Big)\mathrm{d}\zeta\,\mathrm{d}\boldsymbol{x}. \tag{74}$$

It follows that for the right-hand side of (74) to be 0 for all Q_ϵ, we must have (48).

(ii) From (43), (54) and (59), we have that (the leading order contribution to) the total variance of the error is

$$\mathcal{V}(Q) = \tilde{\mathcal{J}}_T(Q) + \mathcal{J}_C(Q) + \mathcal{J}_n(Q). \tag{75}$$

Thus, using (70), (71) and (72), we have

$$\frac{\mathrm{d}}{\mathrm{d}\epsilon}\bigg|_{\epsilon=0}\mathcal{V}(Q+\epsilon Q_\epsilon) \sim 2\,\mathrm{Re}\int \overline{Q_\epsilon}\Big(\int \overline{A}\eta(\mathrm{e}^{\mathrm{i}2\pi \boldsymbol{x}\cdot(\zeta'-\zeta)}QA\eta(\tilde{S}_T + \tilde{S}_C) - \tilde{S}_T\tilde{\chi})\,\mathrm{d}\zeta' + \tilde{S}_n Q\eta\Big)\mathrm{d}\zeta\,\mathrm{d}\boldsymbol{x}. \tag{76}$$

In order for the right-hand side of (76) to be 0 for all Q_ϵ, we must have

$$\int \overline{A}\eta\, \mathrm{e}^{\mathrm{i}2\pi \boldsymbol{x}\cdot(\zeta'-\zeta)}(QA\eta(\tilde{S}_T + \tilde{S}_C) - \tilde{S}_T\tilde{\chi})\mathrm{d}\zeta' + \tilde{S}_n Q\eta = 0. \tag{77}$$

The stationarity assumption on $T-\mu$ and C implies that

$$\tilde{S}_T(\zeta,\zeta') = S_T(\zeta)\delta(\zeta-\zeta'), \tag{78}$$

$$\tilde{S}_C(\zeta,\zeta') = S_C(\zeta)\delta(\zeta-\zeta'). \tag{79}$$

Thus, (77) reduces to

$$\overline{A}\eta[QA\eta - \tilde{\chi}_\Omega]S_T + \overline{A}\eta QA\eta S_C + Q\eta\tilde{S}_n = 0, \tag{80}$$

which can be solved explicitly for Q; this results in (53). That Q satisfies a symbol estimate follows from the assumptions on S_T, S_C and S_n, and from facts about symbol estimates [10–12]. □

The results (48) and (53) tell us how we should design the imaging algorithm to take into account the statistics of the noise, clutter and target.

The multiple of the matched filter (53) can be viewed as an adaptive Wiener filter designed in the Fourier domain. However, unlike the standard time-invariant Wiener filter, it is a time-varying filter in which the filter response varies with respect to $\boldsymbol{x}$, the point reconstructed in the image and s, the point on the flight trajectory.

We see that suppressing clutter and noise comes at a cost, namely that even the leading order term of the bias may be nonzero. This means that although the visible singularities of the estimate $E[\hat{T}]$ are in the correct position and orientation, their strengths may be suppressed. Nevertheless, the strength of the visible singularities of the noise and clutter autocovariance is suppressed so that the mean-square error between the target scene and image is minimized.

We note that when $S_C(\boldsymbol{\xi}) = 0$ and $S_N(\boldsymbol{\xi}) = 0$, the filter Q given in (53) is the same as the one given in theorem 2 and [13].

We note also that (53) can be used in (67) and (75) to obtain explicit expressions for the bias and variance in the stationary case. In addition, (48) and (53) can be used to study waveform design: we can ask which waveform (part of the amplitude A) will result in the best image. This we leave for the future.

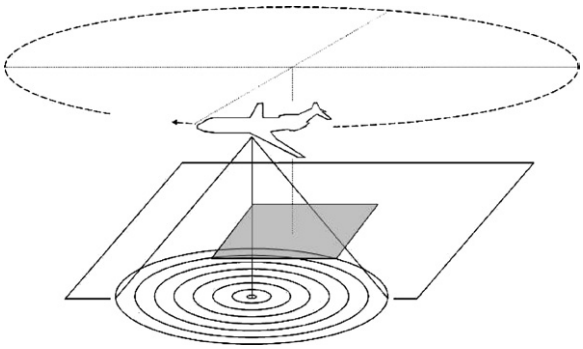

Figure 2. Acquisition geometry used in the numerical simulations. The flight trajectory is a circle with radius 30 km at 15 km altitude. The illuminated region is the disc with diameter 50 km, centred at the origin.

4. Numerical simulations

We performed numerical simulations to demonstrate the performance of the reconstruction methods and to illustrate the theorems. We focused primarily on the case where the filter Q is chosen as in theorems 2 and 3(ii). We also analysed the computational complexity of our method and compared it with the existing algebraic reconstruction methods.

We make the following assumptions in our numerical simulations. We assume that the earth surface is flat. For simplicity we choose $A \equiv 1$; this corresponds to an isotropic antenna radiating a delta-like impulse. We normalize all the distances with respect to the origin by 10 km, i.e. if H denotes the altitude of the flight path then $H = 1.5$ implies that the altitude is 15 km.

We set the flight trajectory to be a circle centred at (25 km, 25 km) with radius equal to 30 km at 15 km above the ground (see figure 2), i.e.,

$$\gamma(s) = (2.5 + 3\cos s, 2.5 + 3\sin s, 1.5), \qquad s \in [0, 2\pi). \tag{81}$$

The region of reconstruction lies within the circle centred at (25 km, 25 km) with radius 25 km where we denote the origin by (0, 0).

The goal of our numerical simulations is to study the performance of the reconstruction algorithm. In order to isolate the algorithm performance from the issue of how to estimate spectral density functions, we choose simple functions to represent the target T and clutter C so that we can use an analytic expression for their power spectral density functions:

$$S_T(\boldsymbol{\zeta}) = \left| \int \mathrm{e}^{-\mathrm{i}2\pi \boldsymbol{x}\cdot\boldsymbol{\zeta}} T(\boldsymbol{x})\, \mathrm{d}\boldsymbol{x} \right|^2, \qquad S_C(\boldsymbol{\zeta}) = \left| \int \mathrm{e}^{-\mathrm{i}2\pi \boldsymbol{x}\cdot\boldsymbol{\zeta}} C(\boldsymbol{x})\, \mathrm{d}\boldsymbol{x} \right|^2. \tag{82}$$

The target is then discretized on a grid and its mean and variance are estimated by the sample mean and sample variance estimators. Realizations of the clutter and noise processes are generated on the discrete grid from a Gaussian white noise process using the Karhunen–Loeve transform based on predefined autocovariance or power spectral density functions.

We define the signal-to-clutter ratio (SCR) and signal-to-noise ratio (SNR) by

$$\mathrm{SCR} = 20\log \frac{\frac{1}{N_T}\sum_1^N (T(\boldsymbol{x}_i) - \mu_T)^2}{E[\|C\|^2]}\ \mathrm{dB}, \tag{83}$$

$$\mathrm{SNR} = 20\log \frac{\frac{1}{N_d}\sum_1^N (d(s_i, t_i) - \mu_d)^2}{E[\|n\|^2]}\ \mathrm{dB}, \tag{84}$$

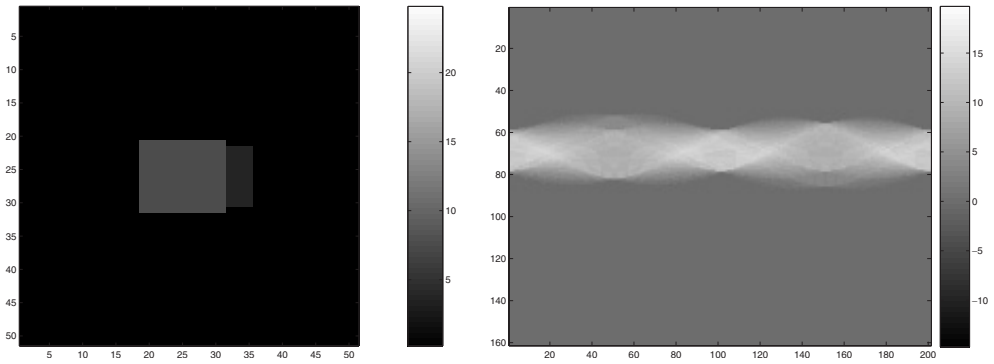

Figure 3. Left: target, right: its radar data, where vertical and horizontal axes correspond to fast and slow time variables t and s, respectively.

where N_T and N_d are the number of grid points and μ_T and μ_d are the mean values of the target scene and its radar data, respectively. We define the mean-square error (MSE) by

$$\mathrm{MSE} = \frac{\sum_{j=1}^{M} \sum_{i=1}^{N_T} |T(\boldsymbol{x}_i) - \hat{T}_j(\boldsymbol{x}_i)|^2}{N_T M}, \tag{85}$$

where $\hat{T}_j$ is the reconstructed image for the jth realization of noise and clutter processes.

We performed three sets of numerical experiments: reconstruction of the target in the presence of (i) clutter only, (ii) noise only and (iii) both noise and clutter . We compared the performance of the filters in theorems 2 and 3(ii) at different SNR and SCR levels. For simplicity, we refer to the filter in theorem 2 as filter Q_1 and the filter in theorem 3(ii) as filter Q_2.

We choose the target scene $T(\boldsymbol{x})$ as

$$T(x_1, x_2) = \tfrac{900}{121}\chi_{[1.8,3]\times[2,3]} + \tfrac{450}{121}\chi_{[3,3.4]\times[2.1,2.9]}, \tag{86}$$

where $\chi_{[a,b]\times[c,d]}$ denotes the characteristic function over the rectangle $[a, b] \times [c, d]$. The target is discretized on a grid of 51×51 which corresponds to a square region of side 50 km with the target in its centre.

From (82), the power spectral density function of the target is

$$S_T(\zeta_1, \zeta_2) = \left| \frac{900}{121} \frac{\sin(1.2\pi\zeta_1)}{\pi\zeta_1} \frac{\sin(\pi\zeta_2)}{\pi\zeta_2} \mathrm{e}^{-\mathrm{i}(4.8\zeta_1+5\zeta_2)} + \frac{450}{121} \frac{\sin(1.4\pi\zeta_1)}{\pi\zeta_1} \frac{\sin(0.8\pi\zeta_2)}{\pi\zeta_2} \mathrm{e}^{-\mathrm{i}(6.4\zeta_1+5\zeta_2)} \right|^2. \tag{87}$$

Figure 3 shows the target scene and its radar data.

We chose the clutter model as a high-frequency version of the target model:

$$S_C(\zeta_1, \zeta_2) = \frac{1}{4} \sum_{\pm} \left(S_T(\zeta_1 \pm 8, \zeta_2 \pm 8) + S_T(\zeta_1 \pm 8, \zeta_2 \mp 8) \right). \tag{88}$$

4.1. Simulations of target in clutter

Figure 4 shows a realization of target embedded in clutter and its radar data when $\mathrm{SCR} = -4$ dB.

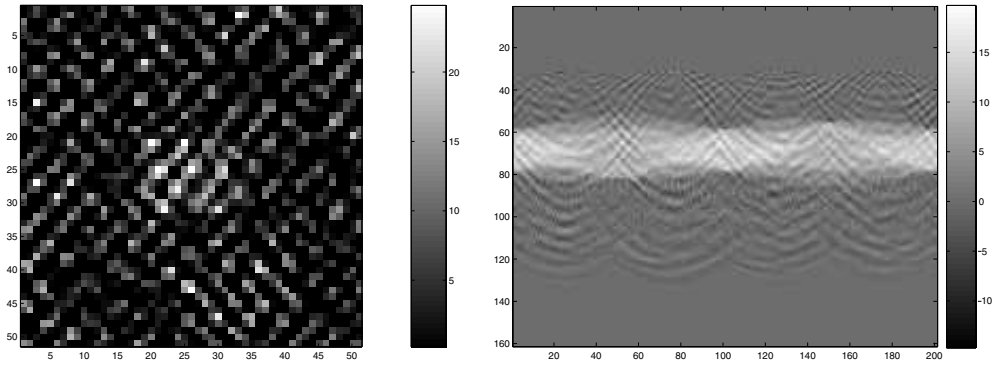

Figure 4. Left: target embedded in clutter, right: its radar data when SCR $= -4$ dB.

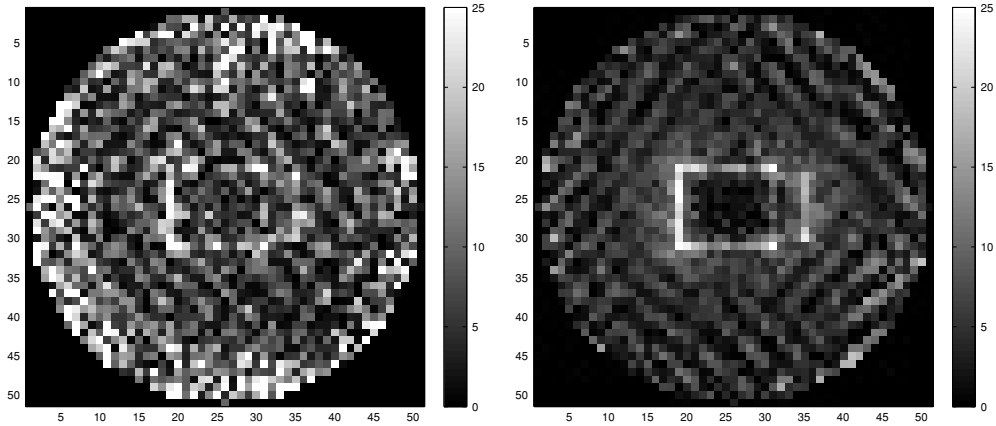

(a) (b)

Figure 5. Left: reconstructed image for single realization of clutter, right: average of ten reconstructed images for different realizations of clutter using filter Q_1 when SCR $= -4$ dB.

Figures 5(a) and 6(a) show the reconstructed images using filters Q_1 and Q_2 for a single realization of clutter, when SCR $= -4$ dB.

We ran simulations to illustrate some of the results stated in the theorems. In particular, theorem 1(i) states that the backprojection operation puts the visible singularities of the mean target scene at the correct location and orientation in the mean value of the estimated image. Theorem 2(i) states that the mean value of the estimated target is unbiased at the singularities. Consequently, we performed ten reconstructions for different realizations of the clutter when SCR $= -4$ dB and averaged the resulting reconstructions. Figures 5(b) and 6(b) show the mean values of the estimated target scene for the two different filters Q_1 and Q_2, respectively. Clearly, in both images, the edges of the target are visible.

Figure 7 shows the MSE of the reconstructed images averaged over ten different realizations of clutter using filters Q_1 and Q_2 at various SCR values. Note that at high SNR values, the performance of the two filters is similar since filter Q_2 approximates filter Q_1 at high SNR.

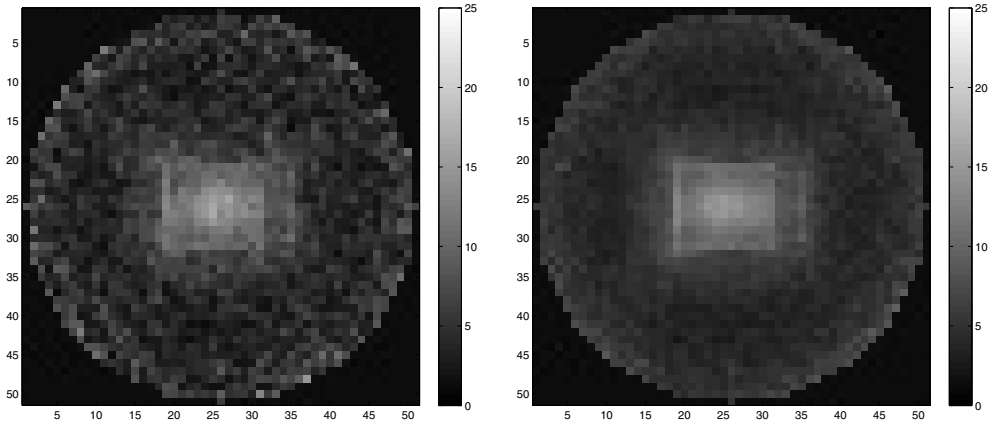

Figure 6. Left: reconstructed image for a single realization of clutter, right: average of ten reconstructions for different realizations of clutter using filter Q_2 when SCR $= -4$ dB.

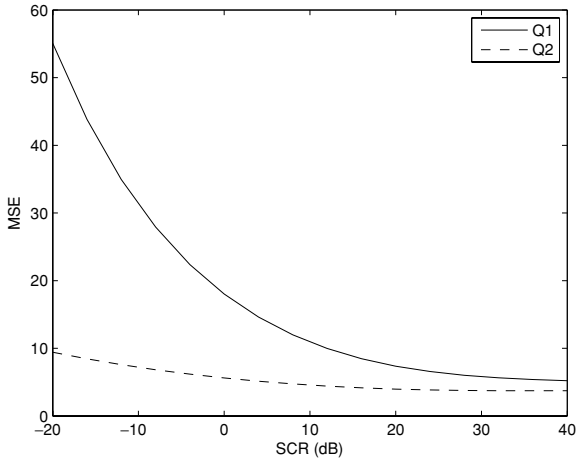

Figure 7. MSE (vertical axis) versus SCR (horizontal axis) averaged over ten reconstructed images for each SCR level using filters Q_1 (solid line) and Q_2 (dashed line).

4.2. Simulations of target in additive noise

Since the transmitted pulse is an ideal wide-band signal, we chose a wide-band noise model which behaves like a $1/f$-type process:

$$S_N(s,\omega) = \frac{1}{1+|\omega|^5}\frac{\pi/5}{\sin(\pi/5)}. \tag{89}$$

Figure 8 shows the radar data of the scene in the presence of noise when SNR $= 10$ dB.

The left-hand sides of figures 9 and 10 show the reconstructed images using filters Q_1 and Q_2, respectively, for a single realization of noise. The right-hand sides show the averaged image over ten reconstructions for different realizations of noise when SNR $= 10$ dB.

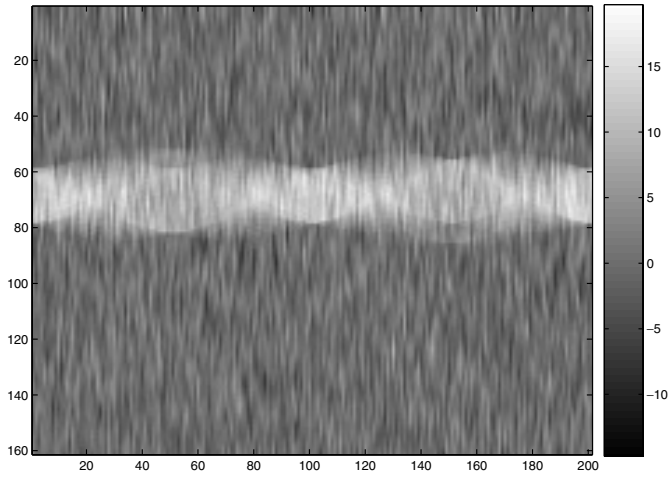

Figure 8. Projection data of the target in the presence of noise when SNR = 10 dB.

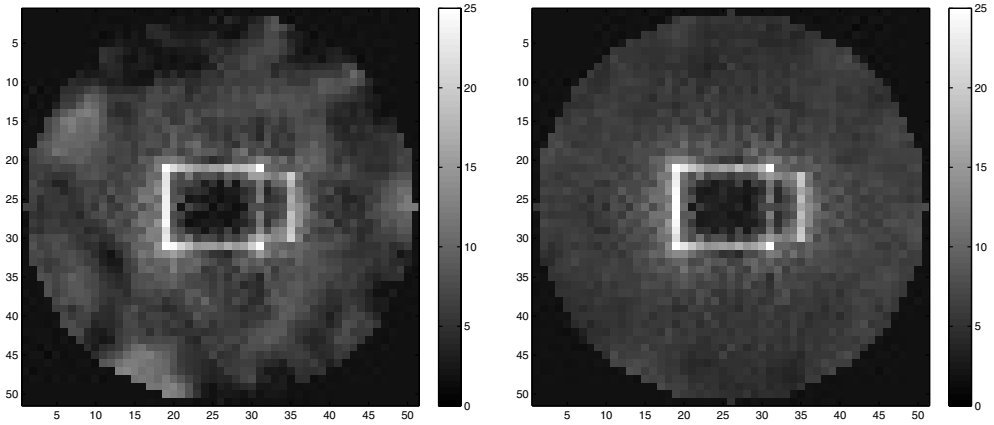

Figure 9. Left: reconstructed image for a single realization of noise, right: average of ten reconstructions for different realizations of noise using filter Q_1 when SNR = 10 dB.

Figure 11 shows the MSE of the reconstructed images using filters Q_1 and Q_2 averaged over ten different realizations of noise at various SNR values. Note that at high SNR values, the performance of the two filters is similar since filter Q_2 approximates filter Q_1 at high SNR.

4.3. Simulations with both clutter and noise

Figure 12 shows the radar data in the presence of both clutter and noise when SCR = −4 dB and SNR = 10 dB.

The left-hand sides of figures 13 and 14 show the reconstructed images using filters Q_1 and Q_2, respectively, for a single realization of clutter. The right-hand sides show the image obtained by averaging ten reconstructions for different realizations of clutter when SCR = −4 dB and SNR = 10 dB.

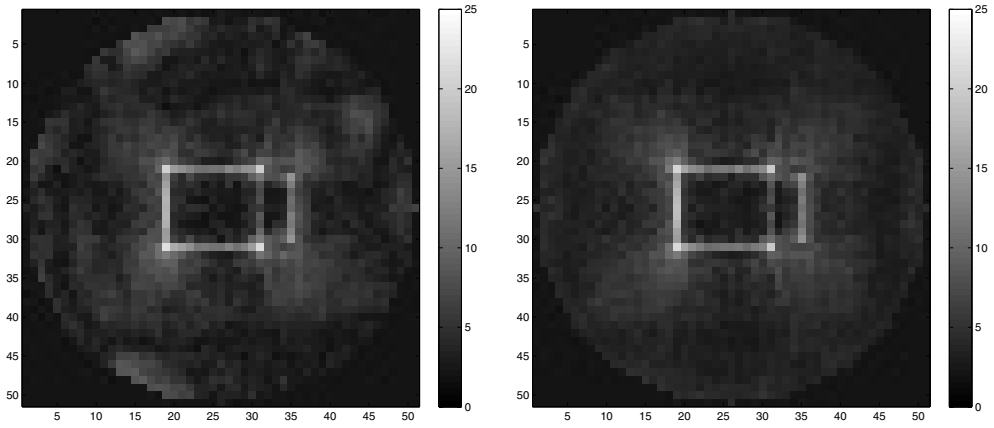

Figure 10. Left: reconstructed image for a single realization of noise, right: average of ten reconstructions for different realizations of noise using filter Q_2 when SNR $= 10$ dB.

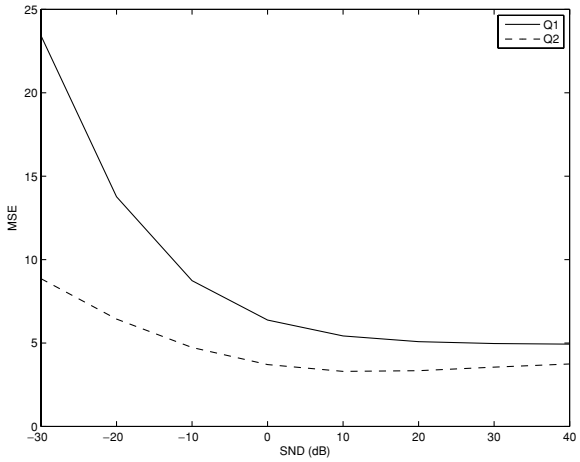

Figure 11. MSE (vertical axis) versus SNR (horizontal axis) averaged over ten reconstructions at each SNR level using filters Q_1 (solid line) and Q_2 (dashed line).

In all three cases, our numerical simulations show that filter Q_2 yields better quality images than that of filter Q_1 both visually and quantitatively. Theoretically, filter Q_1 preserves the strength of the singularities of the target statistics. However, in the presence of clutter and noise, the target singularities are corrupted by the singularities induced by noise and clutter. This is particularly apparent in the low SNR and SCR data. Note that while the reconstruction using filter Q_2 suppresses the strength of the singularities of clutter and noise, it also changes the strength of the singularities of the target in the reconstructed image which can be observed as minor loss of contrast in the reconstructed images.

4.4. Computational complexity of the method

The computational complexity of the present method is determined by the following steps: computing the Fourier transform in the fast time variable, filtering in the Fourier domain and the backprojection operation.

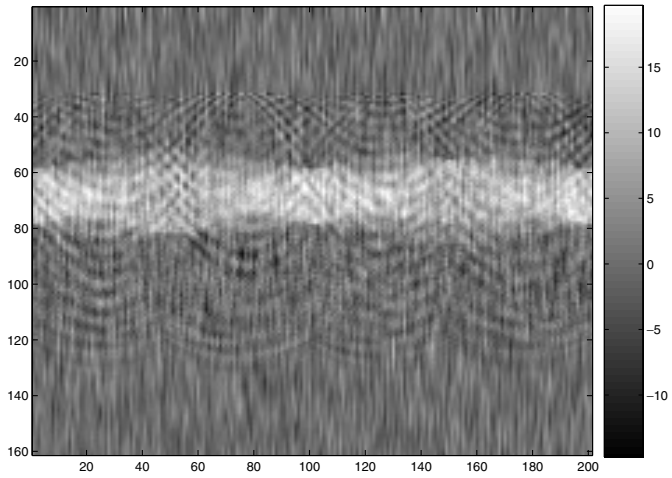

Figure 12. Radar data for target embedded in clutter in the presence of noise, when SCR $= -4$ dB and SNR $= 10$ dB.

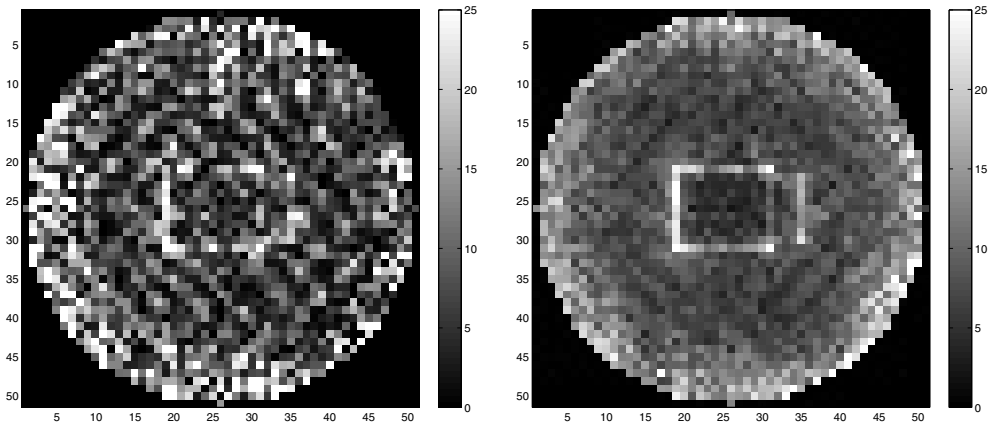

Figure 13. Left: reconstructed image for a single realization of clutter and noise, right: average of ten reconstructions for different realizations of clutter and noise using filter Q_1 when SCR $= -4$ dB and SNR $= 10$ dB.

Assuming that there are $\mathcal{O}(N)$ samples in both the fast time and the slow time variables, the computational complexity of each step is given as follows:

(i) *Computing the Fourier transform in fast time.* Let

$$D(s,\omega) = \int \mathrm{e}^{\mathrm{i}2\pi\omega t}\, d(s,t)\,\mathrm{d}t. \tag{90}$$

For each s, $D(s,\omega)$ can be computed using the fast Fourier transform (FFT) in $\mathcal{O}(N \log N)$ computations. Thus for all s, the computational complexity of the Fourier transform step is $\mathcal{O}(N^2 \log N)$.

(ii) *Filtering in Fourier domain.* Let

$$D_Q(\boldsymbol{z},s,\omega) = D(s,\omega)Q(\boldsymbol{z},s,\omega). \tag{91}$$

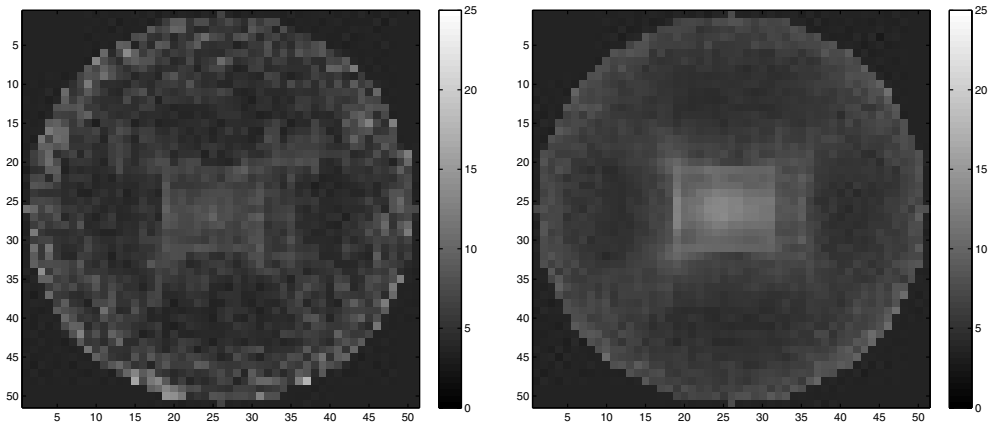

Figure 14. Left: reconstructed image for a single realization of clutter and noise, right: average of ten reconstructions for different realizations of clutter and noise using filter Q_2 when SCR $= -4$ dB and SNR $= 10$ dB.

For an image of size $\mathcal{O}(N \times N)$, computing $D_Q(\boldsymbol{z}, s, \omega)$ requires $\mathcal{O}(N^4)$ operations. If the filter can be factored as $Q(\boldsymbol{z}, s, \omega) = Q_1(\boldsymbol{z}, s)Q_2(s, \omega)$, it would be enough to compute $D_{Q_2}(s, \omega)$, which will reduce the computational complexity of the filtering step to $\mathcal{O}(N^2)$. The multiplication by $Q_1(\boldsymbol{z}, s)$ can be performed in the next step.

(iii) *Backprojection operation.* Finally, we obtain $\hat{T}$ from D_Q by the following backprojection step:

$$\hat{T}(\boldsymbol{z}) = \int D_Q(\boldsymbol{z}, s, \omega)\, \mathrm{e}^{-\mathrm{i}4\pi\omega|r_{z,s}|/c}\, \mathrm{d}\omega\, \mathrm{d}s. \tag{92}$$

The computational complexity of (92) depends on the filtering step (ii). If the filter Q can be factored as in (ii) above D_Q can also be factored as $D_Q(\boldsymbol{z}, s, \omega) = Q_1(\boldsymbol{z}, s)D_{Q_2}(s, \omega)$. Thus, the ω integration can be computed using FFT in $\mathcal{O}(N^2 \log N)$ operations; and the multiplication can be computed in $\mathcal{O}(N^3)$ operations. However, the backprojection has been efficiently implemented in [24, 28] in $\mathcal{O}(N^2 \log N)$ operations. For $\boldsymbol{z}$-dependent filtering, our implementation of (92) is based on direct multiplication and integration, which has a computational complexity of $\mathcal{O}(N^4)$.

Therefore, the computational complexity of our method varies between $\mathcal{O}(N^2 \log N)$ and $\mathcal{O}(N^4)$ depending on the filtering step.

In comparison, the edge-preserving algebraic reconstruction techniques such as the ones presented in [19, 20] use conjugate-gradient-based optimization techniques. For an image of order $\mathcal{O}(N \times N)$, the computational complexity of each iteration in the conjugate gradient method is $\mathcal{O}(N^4)$ [29]. For a convex cost functional, the worst-case scenario requires $\mathcal{O}(N^2)$ iterations for convergence. Thus, the computational complexity of the algorithms in [19, 20] varies between $\mathcal{O}(N^4)$ to $\mathcal{O}(N^6)$.

5. Conclusion

In this paper, we developed synthetic-aperture inversion methods for arbitrary flight trajectory when the data are corrupted with noise and clutter. The methods are based on microlocal analysis. Microlocal analysis has previously been applied primarily to deterministic problems.

To our knowledge, our work is the first attempt to use microlocal techniques in a statistical setting.

We used a physics-based forward model for sensor data. Clutter is modelled as unwanted scatters and noise as additive thermal noise.

We developed explicit backprojection-type inversion methods that preserve the location and orientation of singularities of the target statistics while suppressing the strength of the singularities due to noise and clutter.

We analysed how the singularities of the scene statistics are mapped to the image statistics, using microlocal analysis. In particular, we showed that backprojection operators preserve the location and the orientation of target scene statistics in the reconstructed image.

We developed two backprojection filters: (1) the first filter preserves the strength of the singularities of the first- and second-order statistics of the target scene. However, it also preserves the strength of the singularities of the clutter and noise statistics. (2) The second filter selectively suppresses the strength of the singularities of the noise and clutter statistics relative to the target statistics. This filter can be viewed as an adaptive Wiener filter whose response varies with respect to the point reconstructed in the image and the position on the flight path.

We performed numerical simulations to demonstrate the performance of the reconstruction algorithms. The simulations confirm the properties of the two estimators.

While our present study has focused primarily on SAR, the same approach can be applied to other imaging problems involving Fourier integral operators of the form (1), such as those arising in sonar and geophysics.

We leave for the future the exploration of the theory in situations where our assumptions do not hold.

Acknowledgments

We would like to thank Lizabeth Rachele for reading the original manuscript and for valuable comments, and Gang Xie for developing the first versions of the reconstruction codes. The authors would also like to thank David Donoho, Yoram Bresler and Mujdat Çetin for helpful conversations. We are grateful to Air Force Office of Scientific Research[3] for supporting this work under the agreements F49620-03-1-0051, FA9550-04-1-0223 and FA9550-06-1-0017.

Appendix. Microlocal analysis and image formation

Our image formation algorithm is based on microlocal analysis [10–12], which is the mathematical study of singularities and associated high-frequency structures. It includes the theory of Fourier integral operators and their action on functions with singularities. A Fourier integral operator is an operator with an oscillatory kernel satisfying certain conditions [8, 10–12], of which (1) is an example under assumption (2). The theory for these operators shows how to construct approximate inverse operators, and the resulting inversion algorithms are computationally more efficient than many of the alternatives.

Below we introduce the basic concepts in microlocal analysis.

[3] Consequently, the US Government is authorized to reproduce and distribute reprints for governmental purposes notwithstanding any copyright notation thereon. The views and conclusions contained herein are those of the authors and should not be interpreted as necessarily representing the official policies or endorsements, either expressed or implied, of the Air Force Research Laboratory or the US Government.

A.1. Singularities

The analysis presented here is based on a high-frequency approximation to the imaging system. The study of high frequencies allows us to determine the effect of the imaging system on singularities such as the jump discontinuities between a target and its background. These singularities should appear as edges in the image.

Microlocal analysis considers not only the position (the 'local' information) of a singularity, but also, at each location, the extra ('microlocal') information of the orientation of the singularity. The key microlocal concept, which involves both location and orientation information, is that of the *wavefront set* of a function f.

Definition. The point $(\mathbf{x}^0, \boldsymbol{\xi})$ (in phase space) is not in the *wavefront set* $\mathrm{WF}(f)$ of the function f if there is a smooth cut-off function ϕ that is nonzero at $\mathbf{x}^0$, for which the Fourier transform $F[f\phi](\lambda\boldsymbol{\xi}^0)$ decays rapidly (i.e., faster than any polynomial in $1/\lambda$) as $\lambda \to \infty$, uniformly for $\boldsymbol{\xi}^0$ in a neighbourhood of $\boldsymbol{\xi}$.

In other words, to determine whether $(\mathbf{x}^0, \boldsymbol{\xi})$ is in the wavefront set:

(i) localize f around $\mathbf{x}^0$ (i.e., produce $f\phi$),

(ii) Fourier transform from $\mathbf{x}$ to $\boldsymbol{\xi}$ (i.e., produce $F[f\phi]$),

(iii) look at the decay of the Fourier transform in direction $\boldsymbol{\xi}$.

Example. *A small 'point' scatterer*

Here $f(\mathbf{x}) = \delta(\mathbf{x})$. Since this delta function is supported at the origin, localizing around any point other than the origin results in the function zero, whose Fourier transform, being zero, decays rapidly in all directions. This shows that the location of the only singularity is at $\mathbf{x}^0 = \mathbf{0}$. There remains the question of what directions $\boldsymbol{\xi}$ are in the wavefront set at the origin. To determine these directions, we localize around the origin, thus recovering the original delta function, and then Fourier transform, obtaining a constant. This constant does not decay in any direction; this implies that all directions $\boldsymbol{\xi}$ are in the wavefront set at $\mathbf{x}^0 = \mathbf{0}$. Thus, the wavefront set is $\mathrm{WF}(\delta) = \{(\mathbf{0}, \boldsymbol{\xi}) : \text{all } \boldsymbol{\xi} \neq \mathbf{0}\}$.

Example. *An edge*

An edge of a target might be positioned at the origin, with normal direction $\hat{\boldsymbol{\nu}}$. A model for such a feature is a Heaviside function $H(\boldsymbol{x} \cdot \hat{\boldsymbol{\nu}})$. Localizing around any point $\boldsymbol{x}^0$ for which $\boldsymbol{x}^0 \cdot \hat{\boldsymbol{\nu}} \neq 0$ results in the function 0 or 1, whose Fourier transform decays rapidly in all directions. Thus, the only locations $\boldsymbol{x}^0$ that could be in the wavefront set of H are those for which $\boldsymbol{x}^0 \cdot \hat{\boldsymbol{\nu}} = 0$. To determine which such points are in $\mathrm{WF}(H)$, and to determine the associated directions, we localize around a $\boldsymbol{x}^0$ for which $\boldsymbol{x}^0 \cdot \hat{\boldsymbol{\nu}} = 0$ and Fourier transform. To simplify the calculations, we choose coordinates so that x_1 is along the direction $\hat{\boldsymbol{\nu}}$. Then, the Fourier transform of $\phi(\boldsymbol{x})H(\boldsymbol{x} \cdot \hat{\boldsymbol{\nu}})$ is

$$\int \mathrm{e}^{\mathrm{i}2\pi\boldsymbol{\xi}\cdot\boldsymbol{x}}\phi(\boldsymbol{x})H(x_1)\,\mathrm{d}x_1\,\mathrm{d}x_2 = \int \mathrm{e}^{\mathrm{i}2\pi\xi_1 x_1}H(x_1)\left[\int \mathrm{e}^{\mathrm{i}2\pi\xi_2 x_2}\phi(x_1, x_2)\,\mathrm{d}x_2\right]\mathrm{d}x_1. \tag{A.1}$$

The term in square brackets in (A.1) decays rapidly in ξ_2 because ϕ is smooth and has compact support. Moreover, it is smooth as a function of x_1. The ξ_1-decay of the right-hand side of (A.1) therefore is determined by the jump singularity of H, which implies that (A.1) decays like $(\mathrm{i}\xi_1)^{-1}$. We see that (A.1) decays rapidly in ξ_2 but slowly in ξ_1, which implies that the wavefront set of H is $\mathrm{WF}(H(\boldsymbol{x} \cdot \hat{\boldsymbol{\nu}})) = \{(\boldsymbol{x}, r\hat{\boldsymbol{\nu}}) : \boldsymbol{x} \cdot \hat{\boldsymbol{\nu}} = 0, r \neq 0\}$.

A.2. The pseudolocal property of pseudodifferential operators

A *pseudodifferential operator* is a type of Fourier integral operator, namely an operator

$$\mathcal{L}[u](\boldsymbol{y}) = \int L(\boldsymbol{y}, \boldsymbol{z}) u(\boldsymbol{z})\, \mathrm{d}\boldsymbol{z}, \tag{A.2}$$

in which the kernel L is of the form

$$L(\boldsymbol{y}, \boldsymbol{z}) = \int \mathrm{e}^{\mathrm{i}2\pi(\boldsymbol{y}-\boldsymbol{z})\cdot\boldsymbol{\xi}} A(\boldsymbol{y}, \boldsymbol{z}, \boldsymbol{\xi})\, \mathrm{d}\boldsymbol{\xi}, \tag{A.3}$$

where A satisfies an estimate of the form (2) (see [10–12] for a precise statement). Here, $\boldsymbol{y}$, $\boldsymbol{z}$ and $\boldsymbol{\xi}$ are all in $\mathbb{R}^n$.

Every pseudodifferential operator has the desirable *pseudolocal* property, namely $\mathrm{WF}(\mathcal{L}[u]) \subseteq \mathrm{WF}(u)$. If $\mathcal{L}$ is an image fidelity operator, this means that $\mathcal{L}$ positions singularities at the correct location and preserves their orientation.

To understand why pseudodifferential operators have the pseudolocal property, we consider the following example. Let $u(\boldsymbol{z}) = \delta(\boldsymbol{z}\cdot\hat{\boldsymbol{\nu}}) = \int \mathrm{e}^{\mathrm{i}2\pi \boldsymbol{z}\cdot\hat{\nu}\omega}\, \mathrm{d}\omega$ with $\boldsymbol{z}, \hat{\boldsymbol{\nu}} \in \mathbb{R}^2$, which would correspond, for example, to an edge through the origin with normal direction $\hat{\boldsymbol{\nu}}$. We note that $\mathrm{WF}(u) = \{(\boldsymbol{x}, r\hat{\boldsymbol{\nu}}) : \boldsymbol{x}\cdot\hat{\boldsymbol{\nu}} = 0, r \neq 0\}$.

The operator $\mathcal{L}$ acts on u to produce

$$\begin{aligned}\int L(\boldsymbol{y}, \boldsymbol{z})\delta(\boldsymbol{z}\cdot\hat{\boldsymbol{\nu}})\, \mathrm{d}\boldsymbol{z} &= \int L(\boldsymbol{y}, \boldsymbol{z})\, \mathrm{e}^{\mathrm{i}2\pi \boldsymbol{z}\cdot\omega\hat{\nu}}\, \mathrm{d}\omega\, \mathrm{d}\boldsymbol{z} \\ &= \int \mathrm{e}^{\mathrm{i}2\pi(\boldsymbol{y}-\boldsymbol{z})\cdot\boldsymbol{\xi}} A(\boldsymbol{y}, \boldsymbol{z}, \boldsymbol{\xi})\, \mathrm{e}^{\mathrm{i}2\pi \boldsymbol{z}\cdot\omega\hat{\nu}}\, \mathrm{d}\boldsymbol{\xi}\, \mathrm{d}\boldsymbol{z}\, \mathrm{d}\omega. \end{aligned} \tag{A.4}$$

We make the change of variables $\boldsymbol{\xi} \to \omega\tilde{\boldsymbol{\xi}}$ and apply the method of stationary phase to the $\boldsymbol{z}$ and $\tilde{\boldsymbol{\xi}}$ integrals (dimension $n = 4$, with ω the large parameter). In this calculation, the phase is $\omega[(\boldsymbol{y}-\boldsymbol{z})\cdot\tilde{\boldsymbol{\xi}} + \boldsymbol{z}\cdot\hat{\boldsymbol{\nu}}]$, so the leading order contribution comes from (a) setting to zero the derivative of the phase with respect to $\tilde{\boldsymbol{\xi}}$, which implies that $\boldsymbol{z} = \boldsymbol{y}$, i.e., the location of the singularity is preserved and (b) from setting to zero the derivative with respect to $\boldsymbol{z}$, which implies that $\tilde{\boldsymbol{\xi}} = \hat{\boldsymbol{\nu}}$, i.e., the orientation is preserved. We find that

$$\int L(\boldsymbol{y}, \boldsymbol{z})\delta(\boldsymbol{z}\cdot\hat{\boldsymbol{\nu}})\, \mathrm{d}\boldsymbol{z} = \int A(\boldsymbol{y}, \boldsymbol{y}, \omega\hat{\boldsymbol{\nu}})\, \mathrm{e}^{\mathrm{i}2\pi \boldsymbol{y}\cdot\omega\hat{\nu}}\, \mathrm{d}\omega + \underbrace{\int \mathcal{O}(\omega^{-1})\, \mathrm{e}^{\mathrm{i}\boldsymbol{y}\cdot\omega\hat{\nu}}\, \mathrm{d}\omega}_{\text{smoother}}; \tag{A.5}$$

from the form of (A.5) we see that the wavefront set of $\mathcal{L}[u]$ is $\mathrm{WF}(\mathcal{L}[u]) \subseteq \{(\boldsymbol{x}, r\boldsymbol{\nu}) : \boldsymbol{x}\cdot\boldsymbol{\nu} = 0, r \neq 0\}$. The assumption (2) on A is needed to ensure that the stationary phase calculations do indeed give the leading order term. The leading order and the second term on the right-hand side of (A.5) come from the terms of order $\omega^{-n/2}$ and remainder term of order $\omega^{-n/2-1}$ of the stationary phase theorem. Note that multiplication by ω^m in the integrand can be regarded as a differentiation for $m > 0$ and as an integration for $m < 0$. Therefore, the order ω^{-1} difference makes the second term on the right-hand side of (A.5) one degree smoother than the first term.

We can see from (A.5) that if A is zero at some of the critical points, the corresponding singularities of u could disappear in $\mathcal{L}[u]$. We refer to singularities in u that do appear in $\mathcal{L}[u]$ as *visible* singularities.

References

[1] Curlander J and McDonough R 1991 *Synthetic Aperture Radar* (New York: Wiley)
[2] Cutrona L 1990 *Synthetic Aperture Radar* (New York: McGraw-Hill)
[3] Elachi C 1987 *Spaceborne Radar Remote Sensing: Applications and Techniques* (New York: IEEE Press)

[4] Franceschetti G and Lanari R 1999 *Synthetic Aperture Radar Processing* (New York: CRC Press)
[5] Soumekh M 1999 *Synthetic Aperture Radar Signal Processing with MATLAB Algorithms* (New York: Wiley)
[6] Ulander L and Hellsten H 1999 *Proc. Radar Sensor Technology IV* vol 3704, pp 149–58
[7] Ulander L and Frölund P O 1998 Ultra-wideband SAR interferometry *IEEE Trans. Geosci. Remote Sensing* **36** 1540–50
[8] Nolan C J and Cheney M 2002 Synthetic aperture inversion *Inverse Problems* **18** 221–36
[9] Nolan C and Cheney M 2003 Synthetic aperture inversion for arbitrary flight paths and non-flat topography *IEEE Trans. Image Process.* **12** 1035–43
[10] Duistermaat J J 1996 *Fourier Integral Operators* (Boston: Birkhauser)
[11] Grigis A and Sjöstrand J 1994 *Microlocal Analysis for Differential Operators: An Introduction (London Mathematical Society Lecture Note Series* vol 196*)* (Cambridge: Cambridge University Press)
[12] Treves F 1980 *Introduction to Pseudodifferential and Fourier Integral Operators* vols I and II (New York: Plenum)
[13] Beylkin G 1985 Imaging of discontinuities in the inverse scattering problem by inversion of a causal generalized radon transform *J. Math. Phys.* **26** 99–108
[14] Beylkin G and Burridge R 1990 Linearized inverse scattering problems in acoustics and elasticity *Wave Motion* **12** 15–52
[15] Bleistein N, Cohen J K and Stockwell J 2000 *The Mathematics of Multidimensional Seismic Inversion* (New York: Springer)
[16] Louis A and Quinto E 2000 *Local Tomographic Methods in SONAR* (New York: Springer)
[17] Nolan C J and Symes W W 1997 Global solution of a linearized inverse problem for the acoustic wave equation *Commun. Partial Diff. Eqns* **22** 919–52
[18] Quinto E 1993 Singularities of the x-ray transform and limited data tomography in r^2 and r^3 *SIAM J. Math. Anal.* **24** 1215–25
[19] Çetin M and Karl W C 2000 *Proc. IEEE International Conference on Image Processing* vol 1, pp 701–4
[20] Çetin M, Karl W C and Willsky A S 2002 *Proc. IEEE International Conference on Image Processing* vol 2, pp 481–4
[21] Fessler J 2000 *Handbook of Medical Imaging, Medical Image Processing and Analysis* vol 2, ed M Sonka and J Fitzpatrick (Bellingham, WA: SPIE Optical Engineering Press) pp 1–70
[22] Fawcett J 1985 Inversion of n-dimensional spherical means *SIAM J. Appl. Math.* **45** 336–41
[23] Hellsten H and Andersson L 1987 An inverse method for the processing of synthetic aperture radar data *Inverse Problems* **3** 111–24
[24] Nilsson S 1997 Application of fast backprojection techniques for some inverse problems of integral geometry *PhD Thesis* Linköping Studies in Science and Technology Dissertation No 499
[25] Borden B 1999 *Radar Imaging of Airborne Targets* (Bristol: Institute of Physics Publishing)
[26] Cheney M and Bonneau R 2004 Imaging that exploits multipath scattering from point scatterers *Inverse Problems* **20** 1691–711
[27] Pillai S, Oh H, Youla D and Guerci J 2000 Optimal transmit receiver design in the presence of signal-dependent clutter and channel noise *IEEE Trans. Inf. Theory* **46** 577–84
[28] Ulander L, Hellsten H and Stenström G 2003 Synthetic-aperture radar processing using fast factorized back-projection *IEEE Trans. Aerospace Electron. Syst.* **39** 760–76
[29] Nash S and Sofer A 1996 *Linear and Nonlinear Programming* (New York: McGraw-Hill)